Densities of valence states of amorphous and crystalline III-V and II-VI semiconductors

Nigel J. Shevchik, Javier Tejeda, and Manuel Cardona
Max-Planck-Institut für Festkörperforschung, Stuttgart, Federal Republic of Germany
(Received 24 September 1973)

The densities of valence states (DOVS) of the amorphous and crystalline forms of GaP, GaAs, GaSb, InP, InAs, InSb, AlSb, ZnTe, and CdTe have been determined from the energy-distribution spectra of photoelectrons emitted by high-energy photons (16.9, 21.2, 40.8, and 1486.6 eV). In general the DOVS of the amorphous forms can be represented by a broadened version of those of the corresponding crystalline forms. Fine structure which appears in the upper valence bands of the crystalline materials, due to critical points at L, X, and W, is completely washed out in the amorphous phase. The core-level spectra have nearly the same positions and widths in the amorphous as in the crystalline modifications. This fact indicates that the fluctuations in the Coulombic environment about each type of atom are small, suggesting that the structure is homogeneous and contains an insignificant number of odd-membered rings. The plasma frequencies, determined from the plasma-loss spectra associated with core levels, are the same in the amorphous as in the crystalline phases to within 3%. This fact enables us to conclude that the densities of both modifications differ by less than 6%. We present a simple bond-charge model which can simulate realistically the density of valence states of germanium and zinc-blende-type semiconductors. The valence bands at any point of the Brillouin zone are obtained in this model as the solution of a 4×4 secular equation. Within this model, the structure of the top p-like valence bands depends primarily on overlap between second-neighbor bonds. Thus fluctuations in the position of second neighbors can be invoked to explain the smearing of the fine structure of these bands in the amorphous modifications. A simple model which relates the chemical shifts of the compounds to their ionicity is also discussed.

I. INTRODUCTION

A. Photoelectron spectroscopy and density of valence states

Within recent years the full potential of high-energy photoemission, in particular, of the measurement of the energy distribution of photoemitted electrons, for determining densities of valence states (DOVS) has been realized.[1-20] The fundamental principle of the technique is to excite the electrons with high-energy photons (x rays, far-uv) so as to eliminate distortions produced by structure in the density of final states and in the matrix elements for the excitation.[1] For this purpose excitation with Al $K\alpha$ (1486.6-eV) or Mg $K\alpha$ (1254-eV) photons may seem ideal, except that the intrinsic linewidth of the characteristic $K\alpha_{1,2}$ line limits the resolution to ~1 eV. Even with an x-ray monochromator the resolution is no better than 0.5 eV.[4]

Better resolution (~0.1 eV) is obtained with uv excitation using as a source either synchrotron radiation[5,8,9] or gas-discharge lamps.[12-19] With the discharge lamp, typical lines used are the He I (21.2 eV), He II (40.8 and 48.4 eV), Ne I (16.9 eV) and Ne II (26.9 eV). For a given gas the various lines are well separated and their relative proportion can be changed by adjusting the gas pressure.

There is, however, a basic difference between x-ray (~1000-eV photons) and uv (20–100-eV photons) photoemission. While the escape length of electrons excited with x rays from the valence bands is about 20 Å, that of the corresponding uv emission is considerably less (5–10 Å).[17] There is no question that x-ray photoemission yields bulk properties of reasonably clean samples (one monolayer or less of contamination). In principle, uv photoemission can yield intrinsic distortions in densities of states due to the sampling of surface states.[20,21] Also, extremely clean surfaces (contamination less than $\frac{1}{20}$ monolayer) are required, especially in view of the high uv-photoemission efficiencies of oxides.[16,17]

B. Valence bands of crystalline zinc-blende-type semiconductors

The valence bands of zinc-blende-type semiconductors contain 2 s and 6 p electrons per molecule. The s electrons lie deep in energy (~12 eV) and, in contrast to germanium, there is a gap between these states (labeled III in Fig. 1) and the higher-lying p states. These upper p-like bands split into two groups, the uppermost peak (I in Fig. 1) of nearly pure p character, and peak II of mixed p and s character. We have chosen, for the example of Fig. 1, bands calculated by the self-consistent orthogonalized-plane-wave (SCOPW) method with Kohn-Sham exchange.[22] These calculations are nonrelativistic and thus neglect spin-orbit effects. The main effect of spin-orbit interaction is to split the upper, pure-p-like bands, along the $\Lambda[111]$ and $\Lambda[100]$ directions of the Brillouin zone.

The SCOPW calculations just mentioned[22] belong to the category of the so-called "first-principles" calculations. It is conventional to broaden the meaning "first principles" to include into this category relativistic[23] and nonrelativistic[24] non-self-

consistent OPW, and the muffin-tin-potential calculations [or Korringa-Kohn-Rostoker (KKR) calculations].[25] In the other category of band calculations, the semiempirical ones, several parameters are adjusted so as to fit a selected number of experimental data. Among them are the OPW(adj.),[26] the empirical pseudopotential method (EPM),[27] and the $\vec{k}\cdot\vec{p}$ method.[28,29] It is also conventional in KKR calculations to adjust the height of the muffin tin so as to fit the fundamental gap. Most available DOVS calculations show substantial discrepancies with those obtained from photoemission; these discrepancies increase with increasing ionicity. The only exceptions seem to be the SCOPW calculations of Stukel *et al.*,[22] at least in the cases available for comparison (especially ZnSe).

In Sec. IV B and in the Appendix we present a simple bond model which reproduces the semiquantitative features of the band structures of the germanium and zinc-blende-type semiconductors with a four-function basis set. This model reproduces the strong similarity of the valence bands in all materials of the family, especially that of the top p-like bands which has been known for a long time.[30] In addition, it is able to describe the homopolar and ionic contributions of the crystal potential and the essential effects of second-neighbor overlap, which are expected to be considerably smeared in the amorphous modifications.

C. Amorphous modifications

Amorphous group-IV and -III-V semiconductors are obtained by either vacuum deposition or by sputtering onto substrates at or slightly below room temperature. The II-VI compounds are more difficult to prepare in the amorphous form: according to a recent report,[31] amorphous CdTe and ZnTe are obtained by vacuum deposition onto a substrate held

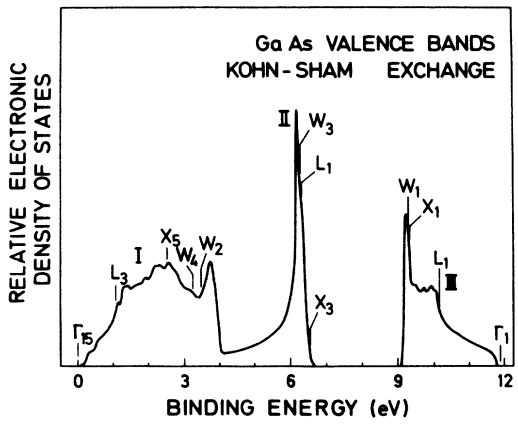

FIG. 1. Density of valence states of GaAs as obtained by the self-consistent orthogonal plane-wave method (SCOPW) with Kohn-Sham exchange (from Ref. 22).

TABLE I. Substrate temperature (°C) used to produce the amorphous and crystalline forms of the III-V and II-VI compounds.

Compound	T_a	T_c
AlSb	20	175
GaP	20	200
GaAs	20	225
GaSb	−50	225
InP	20	225
InAs	−50	225
InSb	−50	100
ZnTe	−150	250
CdTe	−150	200

at 150 °K. Raman scattering and infrared-absorption experiments on Ge and III-V compounds yield first-order spectra very similar to the broadened density of phonon states of the crystalline material.[32-34] This fact suggests a close similarity in the short-range order (i.e., tetrahedral) for both structural forms.[34] The radial distribution functions RDF's, as determined from x-ray diffraction, of sputtered films of III-V semiconductors are rather similar to those of Ge and Si.[35] Because of the similarities in the RDF's, the structural models proposed for amorphous Ge might also be extended to the amorphous III-V compounds.

The continuous random network (CRN) describes rather well the experimental radial distribution functions of Ge and Si.[35-38] Small-angle-scattering experiments[35,39] indicate that the packing efficiency of most amorphous semiconductors is very high, less than 1% of the sample being occupied by voids of radii between 5 and 100 Å, further supporting the validity of the CRN models which are characterized by the following[35-39]: (i) fourfold coordination for every atom, (ii) nearest-neighbor separation within 1–3% of that of the crystal, (iii) a 10° rms bond-angle distortions, (iv) a continuous distribution of dihedral angles between staggered and eclipsed configurations, (v) presence of a large number (20%) of odd-membered rings.

While (i)–(iv) can be fitted into a structural model for a compound semiconductor with no difficulty, (v) cannot. The presence of odd-membered rings in a compound semiconductor requires that bonds between like atoms (wrong bonds) occur, necessarily destroying the chemical ordering. When the model constructed by Polk,[36] is applied to the III-V compounds, at least 10% of the bonds, a sizable number, must be between like atoms.[40] Such bonds could produce a smearing of the electrical and optical properties. In particular, the core-level spectrum should be sensitive to any variations in the Coulombic field brought about by a random charge distribution. We discuss this point in detail in Secs. III and IV C. Because of the wrong-bond

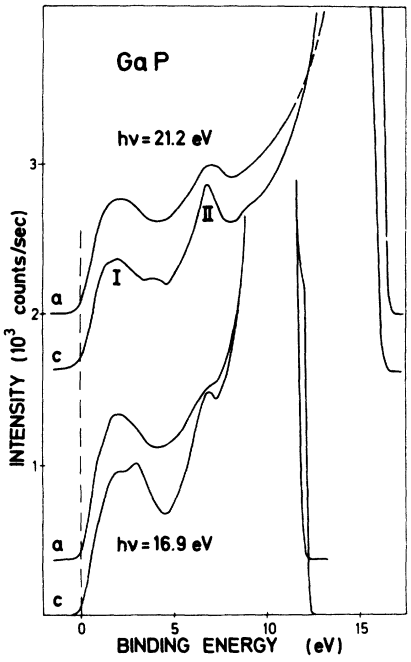

FIG. 2. Electron distribution curves (EDC's) for amorphous (a) and crystalline (c) GaP obtained with photons of $h\nu = 21.2$ and 16.9 eV.

problem encountered in structures containing odd membered rings, structures containing only even-number rings are chemically desirable. If the chemical-bonding discrimination forces are at work during the formation of the films, then we might expect the short-range order of the amorphous III-V compounds to be closer to that of their crystalline forms than that of amorphous Ge.

The optical properties of tetrahedrally coordinated amorphous semiconductors show marked differences with those of their crystalline forms.[41-45] In the fundamental region, the structure in ϵ_2 associated with critical points is destroyed.[45] The ϵ_2 spectra consist of a single peak centered near the energy associated with transitions along Λ in the crystalline form (E_1, $E_1+\Delta_1$). Optical absorption with synchrotron radiation has shown that the structure in the density of conduction states is smeared considerably.[46,47] It is therefore of interest to determine by means of photoemission how much smearing occurs in the valence bands.

D. Theoretical densities of states in amorphous semiconductors

While the electronic properties of crystalline semiconductors are well understood theoretically, this is not the case for amorphous materials. Translational symmetry reduces the calculation of the electronic spectra to a problem involving only the few atoms within the unit cell. For amorphous systems, the unit cell essentially becomes infinite, greatly increasing the number of basis functions needed. The bulk of the theoretical efforts have followed four different approaches: The first is to treat the amorphous form as a perturbation of the crystal[48-52]; the second, to treat small clusters with multiple scattering theory[53-56]; the third, to reduce the complexity of the Hamiltonian to examine the topologically dependent properties[57-59]; and the fourth, to examine crystalline polytypes with large unit cells that approximate the structure of the amorphous form.[60-63] Most of the work has been confined to a-Ge, while little has been done for the amorphous III-V and II-VI compounds. In particular, the effect of wrong bonds which may exist in the amorphous compounds is not known.

The earliest attempt to calculate the electronic spectrum of amorphous Ge was that of Herman and Van Dyke.[48] By assuming that the then reported 30% density deficit of the amorphous form could be represented as a 10% increase in the lattice spacing, they were able to explain the shift in the leading edge of the top of the valence band as determined by Donovan and Spicer.[64] By assuming nondirect transitions, they were able to explain both the red shift and the smearing of structure in the ϵ_2 spectra. Following a similar philosophy, Brust[49] introduced a phonon disorder into the crystal and rescaled the pseudopotential according to a 10–15% density deficit. These approximations resulted in a smearing and red shift of the optical spectra that were in good agreement with experiment. However, it is not clear whether such a smearing pro-

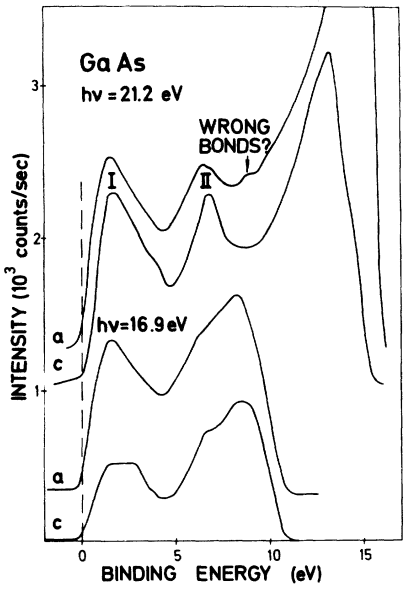

FIG. 3. EDC's for amorphous and crystalline GaAs obtained with photons of $h\nu = 21.2$ and 16.9 eV.

cedure is sufficient to bring the density of valence states into agreement with experiment. Recent photoemission experiments[8,10] show that the width of the valence band of the amorphous form of Ge is the same as that of the crystal. Also, the two-peak structure in the lower valence bands of the crystalline form is washed out in the amorphous form. Several recent structural measurements[35] indicate that the densities and nearest-neighbor spacings of the two structural modifications of Ge and the III-V compounds are the same, which invalidates those procedures rescaling the pseudopotentials.

Kramer *et al.*[50-52] employed a more realistic structural model which includes the loss of long-range order explicitly. This loss introduces a lifetime broadening of the electronic states, which leads to a selective smearing of the optical spectrum, in agreement with experiment. These calculations demonstrate that features associated with the Λ direction are less sensitive to the disorder than those associated with the Δ-direction. However, the smearing is primarily confined to the conduction bands, while the valence bands are essentially the same as in the crystal. Since the lower density of states of the amorphous form of Ge has been shown to be significantly smeared,[8,10] the validity of either the structural model or the calculation procedure in this region is questionable. However, for the amorphous III-V compounds which might have a structure closer to that of the crystal, this procedure may be more valid.

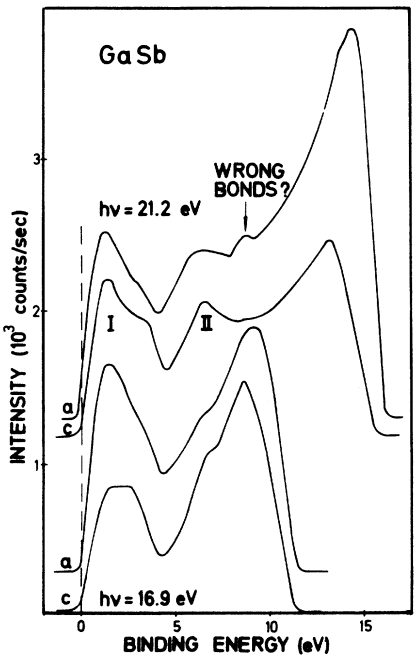

FIG. 4. EDC's for amorphous and crystalline GaSb obtained with photons of $h\nu = 21.2$ and 16.9 eV.

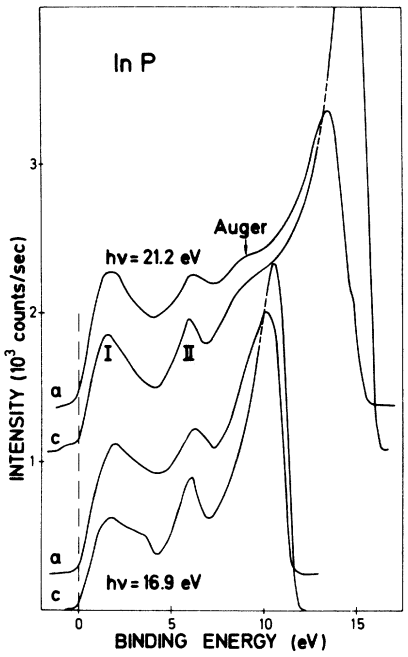

FIG. 5. EDC's for amorphous and crystalline InP obtained with photons of $h\nu = 21.2$ and 16.9 eV.

Another approach to this problem as developed by Ziman and co-workers[53-56] has been to consider multiple scattering from very small clusters. As the size of the cluster increases and a gap begins to form between the valence and conduction states, the calculated electronic properties become more like those of the bulk. With this method, in principle, complex structural configurations including quantitative and topological disorder and the effects of various boundary conditions, can be attacked, but the numerical difficulties in handling very large clusters have not yet been overcome.

Weaire and Thorpe,[57-59] by investigating the properties of a simple Hamiltonian which includes eight orbitals per primitive cell, and nearest-neighbor and atom-splitting overlap parameters, have been able to isolate those features in the density of states that depend upon the short-range order. In particular, they show that the bonding and antibonding p-like bands remain structure-independent δ functions in the density of states, and that the other portions, which are admixtures of p- and s-like functions, are sensitive to the topology of the structure. They reach similar conclusions for III-V compounds as long as they can be represented by two interpenetrating sublattices of the constituent atoms. The destruction of this chemical ordering should obliterate the gap splitting of the lower s-like bands from the upper p-like bands. If the distribution of rings in the amorphous III-V

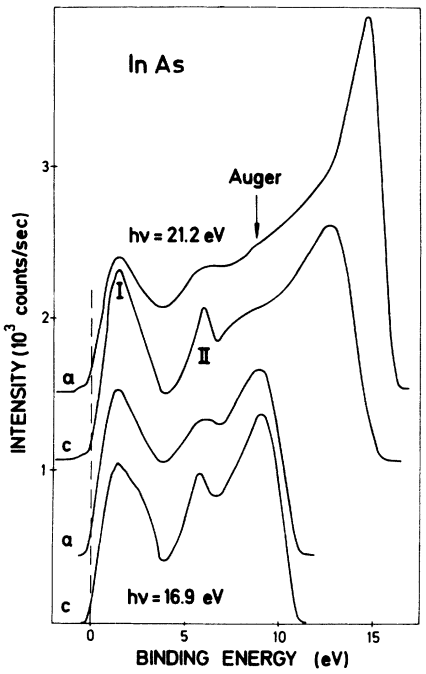

FIG. 6. EDC's for amorphous and crystalline InAs obtained with photons of $h\nu = 21.2$ and 16.9 eV.

compounds is essentially the same as in the crystal, then their theory predicts the DOVS of the two forms to be similar. Any differences should be due to quantitative disorder.

The most notable success of the Weaire-Thorpe theory was their prediction that the lower two-peak structure in the valence bands of cubic Ge should be smoothed into a flat region as a consequence of the odd-membered rings. However, the possibility that quantitative disorder, particularly that induced by second neighbors, can produce a similar smearing was not worked out. The δ-function peaks in the Weaire-Thorpe valence bands are in reality 3- to 4-eV wide,[8,10] signaling that the more distant overlap of π-type bonding is playing a significant role. Henderson and Ortenburger[61] have recently demonstrated that the actual details of the valence and conduction bands can be reproduced with a similar basis set by the inclusion of more distant overlap. We show in the Appendix that the density of valence states of the group IV elements and the III-V compounds can be explained with a four-function basis set, with the inclusion of overlap between second-neighbor bonds. Ortenburger *et al.*[60] demonstrated that the electronic densities of states of the 2*H* and 4*H* polytypes of Ge are similar to those of the cubic form. Also, the density of states and optical spectra of Ge-3, which contains five-fold rings, were strikingly similar to those of amorphous Ge.[62,63] In generalizing this model to a III-V compound one is confronted again with the difficulty of defining the chemical order.

E. Core levels

The electron energy distribution curves yield spectra of all core levels which have binding energies smaller than that of the exciting photon. These binding energies are sensitive to the valence charge distribution and thus may serve as a test of the ionicity of the material, i.e., of electron charge transfer from the cation to the anion. They also can be used to check binding energies of core levels obtained with the SCOPW and other less reliable methods. However, the determination of the binding energies of core levels poses the following difficulties which must be overcome before the core shifts can be meaningfully systematized: (i) chemical shifts produced by oxidized surfaces, (ii) effects of electrostatic charging, (iii) establishment of a reliable origin for the measured binding energies. The "natural" origin, the Fermi level of the sample, varies from sample to sample and often is affected by surface treatment. The top of the valence band, used as a reference in the present work, is a well-defined point and automatically eliminates difficulty (ii). It can be easily referred to the more natural vacuum level by addition of the threshold energy for photoemission (energy gap + electron affinity).

Particularly accurate binding energies and chem-

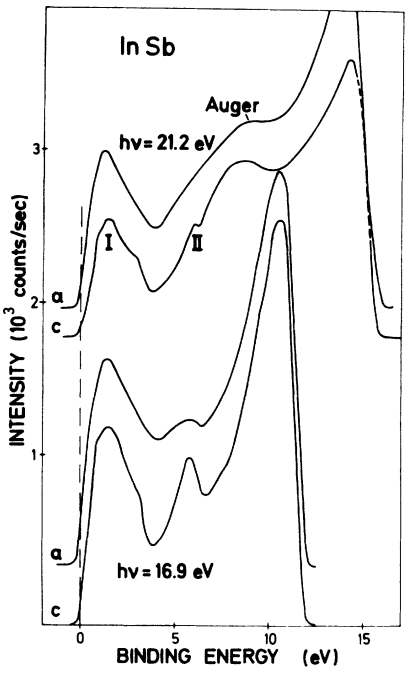

FIG. 7. EDC's for amorphous and crystalline InSb obtained with photons of $h\nu = 21.2$ and 16.9 eV.

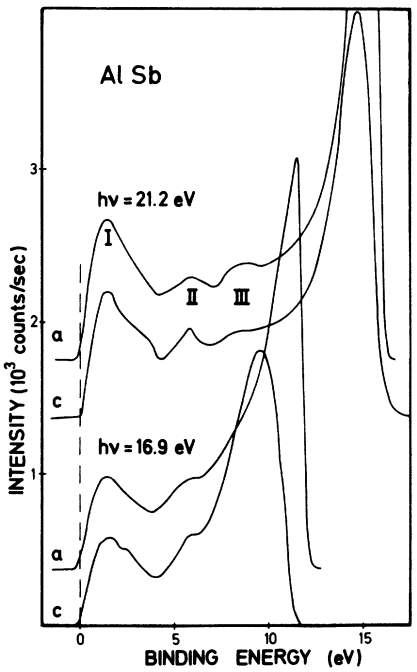

FIG. 8. EDC's for amorphous and crystalline AlSb obtained with photons of $h\nu = 21.2$ and 16.9 eV.

ical shifts for core levels can be obtained with uv photoemission.[65] The binding energies accessible are limited, however, to about 30 eV with gas-discharge lamps (using the He II radiation). These core levels can be easily referred to the top of the valence band which, in the present work, is usually defined to ±0.1 eV. These core levels, exhibiting a linewidth which is not determined by experimental resolution, should provide an excellent test for the presence of wrong bonds in amorphous zinc-blende semiconductors. Broadenings and possibly even splitting of the core lines are expected if a mixture of right and wrong bonds is present.

F. Past photoemission work

Photoemission experiments on Se and GeTe,[12-14,66] have shown that the DOVS of the amorphous form cannot simply be represented as a broadened version of those of the crystal. For the tetrahedrally coordinated semiconductors, most of those experiments concerned with the two structural forms have been limited to Ge and Si.[8,10] The earliest work, performed by Spicer and co-workers[64,67,68] with low-energy photon excitation, found a considerable loss of structure in the electron distribution curves (EDC's) of the amorphous forms of Ge and Si. By assuming the density of conduction states in the amorphous forms of Ge and Si to be flat above the absorption edge, they were able to deduce the top portions of the DOVS. High-energy photoemission experiments of Grobman and Eastman[8] were the first to show that the II and III peaks in Ge and Si were smeared in the amorphous modification. Ley *et al.*, using x-ray photoemission, later confirmed those observations.[10]

Our earlier work performed on AlSb with low-resolution x-ray excitation,[2] showed that the peak II (see Fig. 1) in the DOVS of the amorphous material, is eroded compared to that seen in the crystal, while the gap splitting the p-like states from the s-like states is still retained. It is of interest to examine the amorphous and crystalline forms with higher resolution in order to determine whether any additional smearing occurs beyond the resolution of the x rays.

II. SAMPLE PREPARATION AND EXPERIMENTAL METHOD

The sample preparation and measurements were performed on an ESCA-III system, manufactured by Vacuum Generators, which is equipped with a differentially pumped capillary gas-discharge lamp and an Al $K\alpha$ x-ray source.

The samples were dc sputtered in a high-purity (99.9999%) argon atmosphere at a rate of 2000 Å/h, to about 1 μm in thickness. A base pressure of better than 10^{-7} torr was maintained in the sample preparation chamber with a turbomolecular pump. During sputtering an argon pressure of 30×10^{-3} torr was used. The aluminum substrates were held at temperatures sufficient to produce the desired structural modification (see Table I). Although group IV materials remain amorphous for T_s 300–

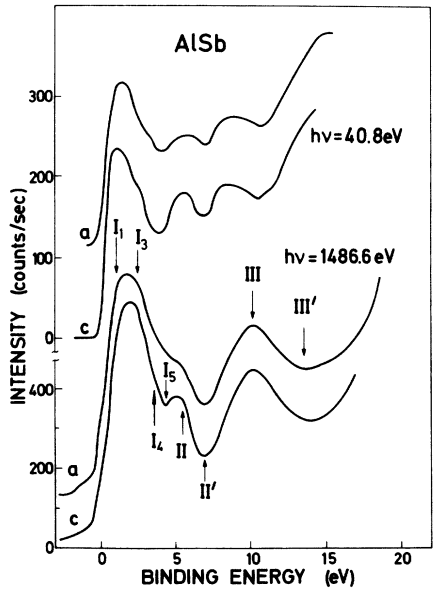

FIG. 9. EDC's for amorphous and crystalline AlSb obtained with photons of $h\nu = 1486.6$ and 40.8 eV.

400 °C, it has been our experience to find that the III-V and II-VI compounds can be produced in their crystalline forms at much lower substrate temperatures.[32,33,35,46,47]

After the samples were sputtered they were brought to room temperature and inserted without breaking the vacuum into the analyzing chamber at better than 5×10^{-10} torr. Chemical contamination by either carbon or oxygen was verified to be absent within the 1-at.% detectability of the x-ray photoemission spectra, corresponding to less than $\frac{1}{10}$ of a monolayer. The samples were then measured with the He I and He II lines ($h\nu = 21.2$ and 40.8 eV) and Ne I line ($h\nu = 16.9$ eV).

To obtain the He I and Ne I lines, the lamp was operated at a high pressure; the gas flow raised the pressure in the analyzing chamber to 1×10^{-9} torr. To obtain the He II line the lamp was operated at a lower pressure; the pressure in the analyzing chamber decreased to 5×10^{-10} torr. The resolution obtained with the He I and Ne I lines was 0.1 eV, and with the weaker He II line, 0.3 eV for the valence bands and 0.1 eV for the stronger core levels. With the x-ray source, the resolution was 1.5 eV for the valence bands and 1.2 eV for the core levels.

III. RESULTS

The photoelectron energy distribution curves (EDC) of the amorphous and crystalline forms of GaP, GaAs, GaSb, InP, InAs, InSb and AlSb, as obtained with 21.2- and 16.9-eV photons, are shown in Figs. 2–8. In Fig. 9 we also show the EDC's of amorphous and crystalline AlSb obtained with 1486.6- and 40-8-eV photons. The EDC's of amorphous and crystalline CdTe and ZnTe, taken with 21.2-eV photons, are shown in Fig. 10; the data for the crystalline forms have been reported elsewhere.[15] All EDC's have been aligned so as to have the onset of emission (top of valence band) coincide with the zero of binding energy. The measurements were performed at room temperature.

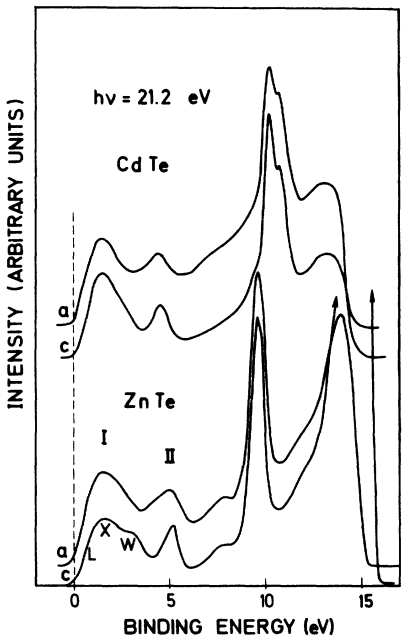

FIG. 10. EDC's for amorphous and crystalline ZnTe and CdTe obtained with photons of $h\nu = 21.2$ eV.

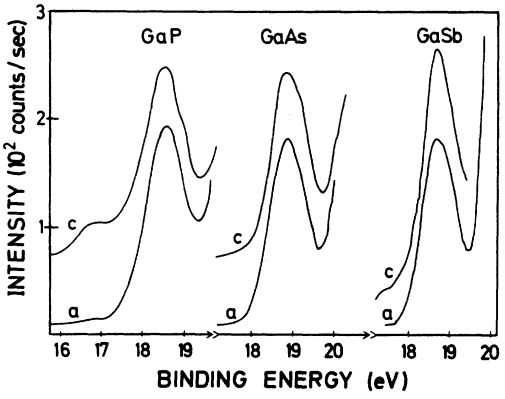

FIG. 11. EDC's from the Ga 3*d* level in amorphous and crystalline GaP, GaAs, and GaSb obtained with $h\nu = 40.8$ eV. The binding energies are referred to the top at the valence band.

Except for the cases mentioned below, the curves are in agreement with those obtained with higher-energy photons by Eastman *et al.*,[8,9] Pollak *et al.*,[3] and Ley *et al.*[69] Taking into account the different matrix elements for the two processes, the x-ray fluorescence measurements of Drahokoupil[70] on GaAs are in agreement with the present photoemission experiments. All curves have a similar prominent peak between 0 and 4.5 eV, labeled I, which arises from the top, *p*-like portions of the valence bands (see Fig. 1). This peak exhibits structure in nearly all crystalline samples but this "fine" structure disappears in the amorphous modifications. The second peak (II) occurs between 4 and 8 eV and exhibits no substructure (one substructure was reported in Ref. 15 for the analogous peak of HgSe). This peak, which corresponds to the second highest, *p*-*s* mixed-valence bands, is broadened considerably in the amorphous modifications. Just below this peak in *a*-GaSb and *a*-GaAs, a small bump occurs which was found to be reproducible for several samples. As we shall discuss later, this peak might be associated with wrong bonds.

In most cases, the emission from the valence bands (peaks I and II) is superimposed upon a secondary tail, which seems to vary in size, depending somewhat on the material involved. The precise

origin of these tails is not well understood, but they are believed to be caused by slight amounts of contamination on the surface of the film. This background seems to be smooth and structureless although it produces a fictitious peak while rising as it encounters the work-function cutoff. The region of peak I and II is not expected to be altered significantly by this secondary background.

For all materials, except AlSb, the lower s-like valence bands (peak III, Fig. 1) could not be seen in the He I and He II spectra. In the He II spectra, the emission from the d levels by the 48.4-eV component obscures them; however, the tops of the valence bands obtained with the 40.8-eV component are in agreement with those obtained from the He I spectra. The s bands may be obscured by final density of states and k-conservation effects (the corresponding conduction states are low), lifetime broadening (the initial states are deep), and small photoionization cross section (a large component of the transitions has $s \rightarrow s$ character). There should be also considerable transfer of oscillator strength from the s to the higher p valence bands. We have estimated this transfer to be about 60%.[15] The peak near the work function cutoff occurs in some cases where we expect peak III to occur, but under these conditions a reliable assignment is not possible.

Peak III can be clearly seen in the x-ray data of Fig. 9 (these results have already appeared in Ref. 2) between 7 and 12 eV with the maximum at 10 eV. Obviously, most of the arguments given above to explain the suppression of peak III with uv excitation do not hold for x rays. We notice that for AlSb, peak III, while weaker, can also be seen in the 21.2- and 40.8-eV curves of Figs. 8 and 9 but it

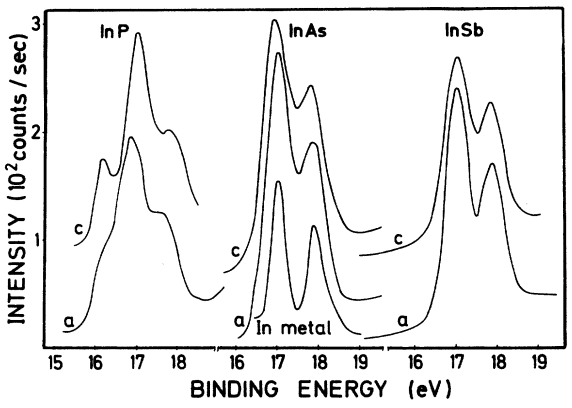

FIG. 12. EDC's from the In 4d level in amorphous and crystalline InP, InAs, and InSb obtained with photons of $h\nu = 40.8$ eV. The binding energies are referred to the top of the valence band. Also included is the EDC from the In 4d level in the metal. This curve has been displaced and aligned with that of InAs for display purposes.

TABLE II. Position of the cation d levels measured with respect to the top of the valence band E^{TVB} and vacuum level E^V. Also included are the spin-orbit splitting ΔE_{so}. All units are eV.

	E^{TVB} $J=\frac{5}{2}$	E^{TVB} $J=\frac{3}{2}$	E^V $J=\frac{5}{2}$	E^V $J=\frac{3}{2}$	ΔE_{so}
GaP	18.6	19.0	24.3[a]	24.7[b]	0.4 ± 0.1
GaAs	18.7	19.1	24.2	24.6	0.4 ± 0.1
GaSb	18.8	19.2	23.6	24.0	0.4 ± 0.1
InP	17.1	17.88	22.8	23.58	0.78 ± 0.02
InAs	16.9	17.72	22.2	23.02	0.82 ± 0.02
InSb	17.1	17.94	21.9	22.74	0.84 ± 0.02
In	17.15	18.07	21.2	22.45	0.91 ± 0.03
Ga[b]	18.4		22.5		

[a]Work function for InP used.

[b]From G. Leonhardt, A. Berndtsson, J. Hedman, M. Klasson, R. Nilsson, and C. Nordling (unpublished).

peaks about 1 eV below the corresponding x-ray peak. An explanation could be that the bottom of band III occurs at $k = 0$ and is s-like. Thus, as mentioned above, it contributes little to the uv excitation. At the edge of the zone the bands become slightly admixed with p states and therefore the cross section would be expected to increase. This may produce a deformation of peak III as seen with uv excitation with respect to that of the x-ray peak, which apparently reproduces faithfully the density of states. This deformation would enhance the lower binding energy and suppress the higher binding energy portions of peak III. We also note that in the 21.2-eV curve of Fig. 8, peak III appears stronger in the amorphous than in the crystalline phase—a possible result of disorder-induced s-p admixture. Surface states, which might form in regions of energy in which a gap appears in the bulk density of states, may also be contributing to discrepancy between the uv and x-ray data. Owing to the shorter escape depth of electrons emitted by uv photons, the uv data are more sensitive to surface states than the x-ray data. Similar discrepancies for uv and x-ray spectra have been observed for the s-like valence peak of Se.[13,14]

We do note some discrepancies between the curves obtained for the 21.2- and 16.9-eV lines. They are most apparent for the crystalline Ga compounds, where the first peak has a flat top only for $h\nu = 16.9$ eV. Such a flat top is not observed in the amorphous form for all excitation energies. We believe that structure in the density of final states and $\vec{k}$ conservation is responsible for this. In the amorphous form there is no $\vec{k}$ conservation and the density of final states has insufficient structure to distort the emission curves. The data taken for the In compounds show a difference at 7–8-eV binding energy for the two photon energies. The differences are particularly large for InSb. This is be-

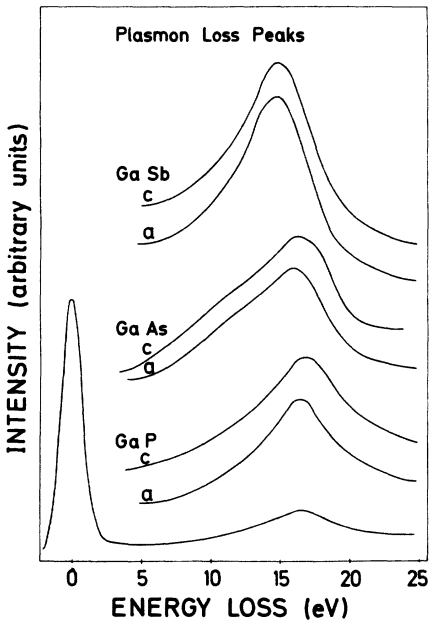

FIG. 13. Plasmon-loss peaks following the emission from the Ga 3*d* level in amorphous and crystalline GaP, GaAs, and GaSb.

cause of the contribution from the Auger electrons produced by the hole excited in the In 4*d* level. This hole is excited with 21.2 but not with 16.9-eV radiation.

For InP and InAs the Auger emission is weaker.

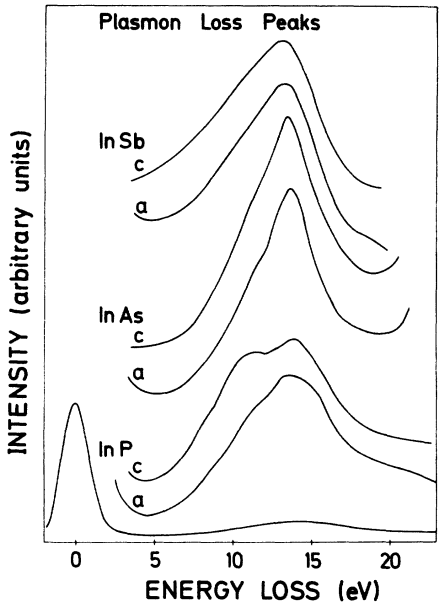

FIG. 14. Plasmon-loss peaks following the emission from the In 4*d* level in amorphous and crystalline InP, InAs, and InSb.

The average valence–conduction-band separation of these materials is about 1 eV higher than in InSb. Thus the photoionization cross section for the In 4*d* levels should be smaller since we are getting a higher proportion of $d \rightarrow s$ transitions. In addition, the valence charge distribution is more localized around the anion in InP and InAs than in InSb because of the higher ionicity and the smaller atomic radius of the anion. It is therefore less likely that Auger transitions involving the cation core and the valence cloud around the anion take place.

Energy distribution curves corresponding to the Ga 3*d* level in amorphous and crystalline GaP, GaAs, and GaSb, excited with 40.8-eV photons, are shown in Fig. 11 with the origin of binding energies taken to be the top of the valence band. Similar curves are shown in Fig. 12 for the In 4*d* level in InP, InAs, and InSb. We first discuss the phosphides since they exhibit shapes markedly different from those of the other materials. For InP, the spin-orbit split peak of the amorphous form has a shoulder at the low binding energy side; in the crystalline form, this shoulder becomes a peak. Similarly in the crystalline form of GaP, we find a small peak at 2-eV lower binding energy. We believe this additional structure to be from phase separated metal, since it lies in the kinetic energy region expected for the pure metal.

Apparently, we are unable to sputter stoichiometric films of the phosphides: some of the highly volatile phosphorus is lost in the process. As the substrate temperature is increased in order to crystallize the material, the amount of segregated metal becomes larger. Hence the amorphous films, particularly GaP, seem to have a better stoichiometry. We wish to emphasize the analytical capabilities of high-energy photoemission to detect such compositional structure. In light of this work, we

TABLE III. Plasmon energies of the amorphous and crystalline forms of the III-V compounds determined from the loss peaks following the emission from the uppermost core levels. All units are eV.

Compound	$\hbar\omega_{pc}$	$\hbar\omega_{pa}$	$\hbar\omega_{fe}$ [a]	$\hbar\omega_{po}$ [b]	$\hbar\omega_{el}$ [c]
AlSb	14.8	14.8	14.0		
GaP	16.8	16.3	16.6	16.9	16.5
GaAs	16.0	15.9	15.5	14.7	15.7
GaSb	14.9	14.7	14.0		14.3
InP	13.9	13.7	14.3		
InAs	13.7	13.7	14.0	13.0	13.8
InSb	13.2	13.3	12.7	12.0	12.8

[a] Free-electron value: $\omega_p = (4\pi ne^2/m)^{1/2}$.

[b] Optical measurements from A. R. Phillip and H. Ehrenreich, Phys. Rev. 129, 1550 (1963).

[c] Energy-loss measurements from C. Festenburg, Z. Phys. 214, 464 (1968).

should suspect any work, particularly the absorption spectra, performed on sputtered phosphide films. The p-p vibrations reported in the Raman spectra of evaporated amorphous InP films[32] suggest a similar mechanism with an excess of phosphorus, contrary to the defect found in the sputtered films. For the arsenic and antimony compounds no such splitting of the d levels occurred, confirming that the films remain stoichiometric to about 2%: The peaks in the amorphous form are as sharp as in the crystalline form. For c-GaP and c-GaAs, we observe shoulders on the low-kinetic-energy side which are probably due to spin-orbit splitting of the Ga 3d levels. For GaSb, we do not see such a splitting. The spin-orbit splitting of the In-4d level is better resolved for In metal than for InSb and InAs. The broadening in the compounds might be caused by the variations in the Madelung sums for atoms lying near the surface.

The position of these core levels with respect to the top of the valence band and the vacuum level are listed in Table II. The positions determined in this way are believed to be accurate to within ±0.2 eV, the primary source of error being the definition of the onset of emission. Also listed in Table II are the spin-orbit splittings of these d levels. Because the $j=\frac{5}{2}$ and $j=\frac{3}{2}$ components of the In 4d level are well resolved, we have been able to estimate its spin orbit splitting to within ±0.02 eV. Compared to the value found in the metal, the spin-orbit splitting of this level decreases by ~10% in the compound. Similar but more dramatic observations have been made for the Zn 3d and Cd 4d levels in the chalcogen compounds.[15]

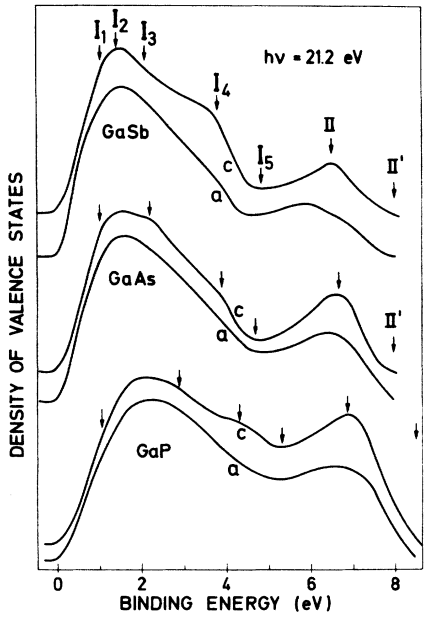

FIG. 15. Peaks I and II of the density of valence states of the amorphous and crystalline forms of GaP, GaAs, and GaSb as obtained from the EDC's with $h\nu=21.2$ eV.

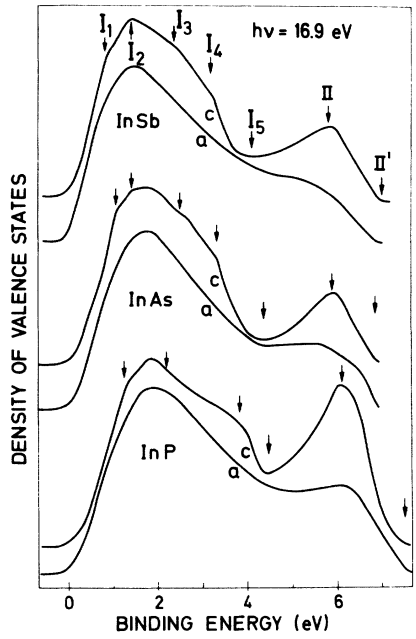

FIG. 16. Peaks I and II of the density of valence states of the amorphous and crystalline forms of InP, InAs, and InSb as obtained with $h\nu=16.9$ eV.

The plasmon-loss peaks following the Ga 3d level in the amorphous and crystalline forms of the gallium compounds, as obtained with 1486.6-eV photons, are shown in Fig. 13. Similar data following the In 4d level are shown in Fig. 14. The zero loss energy is made to correspond to the center of the elastic emission peak from the respective d levels. The plasma energies obtained by this method are

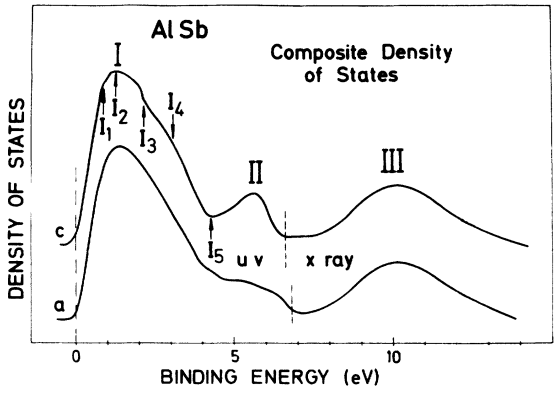

FIG. 17. The complete density of valence states of the amorphous and crystalline forms of AlSb. This is a composite curve using for peaks I and II the EDC for $h\nu=21.2$ eV and for peak III, the EDC for 1486.6 eV.

TABLE IV. Energies (in eV) of features in the density of valence states of GaP, GaAs, and GaSb obtained from EDC's and from band calculations.

	GaP							GaAs								GaSb					
	a	b	c	d	e	f	h	a	b	c	d	e	f	g	h	a	b	d	e	f	h
$I_1; L_3$	1.1	1.15	0.8	1.2	0.8	0.9	1.0	0.8	1.2	0.8	1.4	0.9	1.0	1.0	1.0	1.0	1.0	1.3	1.15	1.1	0.7
$I_2; L_3$					0.9							1.1				1.4	1.4		1.55		
$I_3; X_5$	3.2	2.9		2.7	2.3	2.3	2.4	2.9	2.2	···	2.5	2.6	2.3	2.5	2.3	2.65	2.1	2.7	2.5	2.4	1.7
$I_4; W_2$	4.1	4.3		3.6				3.9	3.9		4.0			3.4		3.8	3.8	2.6	3.1		
$I_5; \Sigma_1$	5.0	5.3	4.1	4.0	3.4	···	3.9	4.5	4.7	4.1	4.4		3.6			4.8	4.8	3.8	3.9		
$II; W_1$	6.7	6.8	···	6.5	···	···	···	6.7	6.7		6.6					6.5	6.5	6.4	6.7		
$II'; L_1$					7.4							7.5							7.3		
$II'; X_3$	8.0	8.5	6.9	6.9	7.2		7.4	8.0		6.9	7.1	7.7	6.3	6.6			8.0	6.9	8.0	6.3	

[a] $h\nu = 16.9$ eV, present work.
[b] $h\nu = 21.2$ eV, present work.
[c] Synchrotron radiation (Ref. 9).
[d] X-ray excitation (Ref. 69).
[e] $\vec{k} \cdot \vec{p}$ calculations (Refs. 28 and 29).
[f] OPW calculations (Ref. 24).
[g] Self-consistent OPW calculations (Ref. 22).
[h] Pseudopotential calculations (Ref. 27).

listed in Table III. Those of the amorphous and the crystalline modification of a given material agree to within 3%. They also agree rather well with the values obtained from the lattice constant using the free electron expression (see also Table III). We can therefore conclude that the densities of both modifications differ by less than 6%, which is smaller than the usual 10% density deficit reported by Stuke and Zimmerer.[45] The differences might be accounted for by the different preparation techniques.

The plasma-loss curve of crystalline InP, and to a lesser extent that of the amorphous modification, shows a shoulder at 11 eV which is probably due to the segregated In excess. The agreement of our measured plasma frequencies with energy-loss measurements of Festenburg is very good. In Fig. 15, we have plotted the DOVS (peaks I and II) derived from the EDC's of GaP, GaAs, and GaSb for $h\nu = 21.2$ eV, after subtracting the secondary-electron background. In Fig. 16 the analogous DOVS are given for the In compounds, obtained from the EDC at 16.9 eV. In contrast to the Ga compounds no strong final-state effects seem to appear in the In compounds at 16.9 eV, and the curves show somewhat better resolution. We have labeled in Tables IV–VI the structure of the crystalline materials according to the critical points of the DOVS calculated by Stukel *et al.*[22] (see Sec. IV). In Fig. 17 we present analogous results for AlSb using the EDC obtained with 21.2-eV photons for peaks I and II and with 1486.6 eV for peak III.

IV. DISCUSSION

A. Density of valence states in crystalline and amorphous materials

We shall now try to interpret the DOVS of the measured crystalline materials in terms of the calculated DOVS of Fig. 1 and other calculations. It has been shown that the self-consistent OPW DOVS of Fig. 1 is that which agrees best with photoemission experiments, especially for highly ionic materials.

Peak I in Fig. 1 starts at the Γ_{15} point with zero binding energy (M_0 critical point). It then climbs and exhibits an M_1 critical point at L_3. An M_2 critical point follows at $X(X_5)$ and then some structure related to the flat-top bands along the W-K direction. The I bands plummet to zero at K or at a Σ point near K. The L_3-X_5 critical points are very close and, with natural broadening, they nearly blend together into a rounded top of the type shown in Figs. 15–17. There is, therefore, some arbitrariness in the choice of these L_3 and X_5 critical points energies from the data of Figs. 15–17. We take the L_3 point (labeled I_1) to be the sharpest feature at the low-energy side of peak I (see GaAs, Fig. 15) and X_5 the point (labeled I_3) of largest curvature at the high-binding-energy side. Actually, in materials with heavy anions (antimonides, tellurides, possibly arsenides) the L_3 point splits owing to spin-orbit interaction and a corresponding structure should be expected at peak I. We labeled these spin-orbit-split critical points I_1-I_2. They appear rather clearly in InSb (Fig. 16), GaSb (Fig. 15), AlSb (Fig. 17), ZnTe, CdTe (Fig. 10), and possibly InAs (Fig. 16). The feature due to the flat-top valence bands along the W-K line has been observed in all our crystalline samples. It is labeled I_4 in the figures and in Tables IV–VI.

We also list in these tables the energy of the minimum which separates peaks I and II (this minimum, labeled I_5, corresponds to the Σ_1, M_3 critical point), that of peak II and that of the minimum following peak II (II′). Peak II is produced by the nearly isotropic second-lowest valence bands (most iso-

TABLE V. Energies (in eV) of features in the density of valence states of InP, InAs, and InSb obtained from EDC's and from band calculations.

	InP						InAs						InSb					
	a	b	d	e	f	h	a	b	d	e	f	h	a	b	c	d	e	f	h
I_1; L_3	1.1	1.0	1.0	0.8	0.6	0.8	1.1	1.0	0.9	0.8	0.7	0.7	0.85	0.9	1.05	1.4	1.0	0.8	0.6
I_2; L_3				0.95			1.45	1.35		1.0			1.35	1.35			1.4		
I_3; X_5	2.2	2.1	2.0	2.3	1.7	1.7	2.	2.3	2.4	2.0	1.8	1.8	2.35	2.3		2.4	1.9	1.9	2.3
I_4; W_2	3.8	3.5	2.5				3.3	3.2	2.7				3.2	3.0		3.1			
I_5; Σ_1	4.4	4.2	3.2			3.0	4.3	4.1	3.3	2.9			4.1	4.0	3.65	3.4	2.7		
II; W_1	6.0	6.0	5.4				5.9	6.0	5.8	6.9			5.8	6.1	•••	5.9	6.1		
II'; L_1				7.6						6.9							6.0		
II'; X_3	7.3	7.1	5.9	7.7	4.5		6.8	6.	6.3	7.4		5.2	7.0		6.5	6.4	6.7	5.0	

[a] $h\nu = 16.9$ eV.
[b] $h\nu = 21.2$ eV (present work).
[c] Synchrotron radiation (Ref. 9).
[d] X-ray excitation, (Ref. 69).
[e] $\vec{k}\cdot\vec{p}$ calculations (Refs. 28 and 29).
[f] OPW calculations (Ref. 24).
[h] Pseudopotential calculations (Ref. 27).

tropic along the W-K lines which thus correspond to maximum II) and therefore shows in Fig. 1 a shape very similar to the DOVS of a one-dimensional band. The cutoff of this peak II′ is either an L_1 or an X_3 point. For AlSb we have also observed with x rays and listed in Table VI the s-like peak III and its cutoff III′ (Fig. 17).

For the sake of comparison we have also listed in Tables IV–VI the results of some measurements by Eastman and co-workers using synchrotron radiation[8] and those of Ley *et al.* using a monochromatized Al $K\alpha$ source.[69] The critical-point energies obtained from several band-structure calculations ($\vec{k}\cdot\vec{p}$,[28,29] self-consistent OPW,[22] non-self-consistent OPW,[23,24] pseudopotential[27]) are also listed.

We note that the observed I_1-I_2 spin-orbit splitting for the antimonides (0.4–0.5 eV) and for the tellurides (0.4–0.6 eV) is in reasonable agreement with that value obtained from the interband optical spectra.[71] After removing this spin-orbit splitting, the L_3 point occurs in all measured materials 1.1–1.2 eV below the top of the valence band, an empirical fact which has been known for over ten years.[72] Surprisingly, many band calculations, including all listed in Table VI for ZnTe and CdTe, give much smaller binding energies for the L_3 point. The self-consistent OPW calculations, however, give 1.0 eV for GaAs and 1.2 eV for ZnSe, in good agreement with experiments. The X_5 point occurs between 2 and 2.5 eV for all compounds, an energy also larger than predicted by band calculations but somewhat smaller than the value of 3.0 eV suggested empirically by Hilsum.[30] The ratio of the binding energy of the X_5 to that of the L_3 point is close to 2 in most materials, a value predicted independently of material by our simple band model discussed in the Appendix.

Similar discrepancies between experiments and band calculations exist for peak II and threshold II′: The experiment energies are larger than the calculated ones and this disagreement seems to increase with ionicity. Reasons for the discrepancies of the various computational methods have been suggested elsewhere.[15]

In contrast to the situation found in Ge, the DOVS of the amorphous forms of the III-V and II-VI compounds can be well generated by a uniform broadening of the DOVS of the crystalline form. This is in agreement with the predictions of Kramer, Maschke, and Thomas,[50–52] although the degree of smearing observed is significantly greater than predicted. Since the onset of the emission remains as sharp in the amorphous as in the crystalline form, the smearing near the Γ region is small. Peak I is broadened on its low-energy side: the valley separating it from peak II is not as deep as in the crystalline form. Peak II appears to be the

TABLE VI. Energies (in eV) of features in the density of valence states obtained from EDC's and from band calculations for AlSb, ZnTe, and CdTe.

	AlSb						ZnTe				CdTe					
	a	b	d	e	f	h	b	d	f	h	b	c	d	e	f	h
I_1; L_3	0.95	0.9	1.0				0.8	1.1	0.6	0.5	1.0	0.7	0.9	0.6	0.4	0.4
I_2; L_3	1.45	1.3					1.4				1.4			1.0		
I_3; X_5	2.1	2.0	2.3	2.4	2.1	1.8	2.3	2.4	1.5	1.0	2.0		1.8	1.0	1.1	1.0
I_4; W_2		3.5	3.6				3.2	2.7			2.7		2.2			
I_5; Σ_1	4.3	4.3	4.5			2.7	4.1	3.2			3.5		2.7	1.9		
II; W_1	5.65	5.8	5.5				5.2	5.1			4.6		4.5			
II'; L_1				6.7						3.6						3.0
II'; X_1	6.50	6.75	7.2	6.4			6.1	5.5	3.7	3.8	5.6		5.1			2.8
III; L_1				9.2	8.5											
III; X_1		8.3	10.0	8.5	7.8											
III'; Γ_1		10.5	12.0	12.7	10.1											

[a] $h\nu = 16.9$ eV (present work).
[b] $h\nu = 21.2$ eV (present work).
[c] Synchrotron radiation (Ref. 9).
[d] X-ray excitation (Ref. 2) and (Ref. 69).
[e] $\vec{k} \cdot \vec{p}$ calculations, [Ref. 28 and same authors (unpublished)].
[f] OPW calculations, (Ref. 24).
[h] Pseudopotential calculations (Ref. 27).

most sensitive to the disorder, but this may be an optical illusion due to its greater sharpness relative to peaks I and III in the crystalline form. However, this peak arises from regions at the band edges and should be more sensitive to the disorder. Weaire and Thorpe[59] have argued that this peak is sensitive to disorder, especially to wrong bonds, since it depends upon nearest-neighbor overlap. Peak III is already broadened so much by lifetime effects in the crystalline form that it is difficult to detect any additional disorder-induced broadening.

The gap splitting peaks II and III is well maintained in amorphous AlSb. Because of lifetime broadening and secondary electrons, it is difficult to detect tailing into the gap region induced by disorder effects. Weaire and Thorpe[59] have argued that this gap should be sensitive to the chemical ordering; the maintenance of this gap indicates a high degree of chemical ordering (i.e., no more than 10% of the bonds are wrong). However, for GaAs and GaSb, the small bump observed in the gap region could be produced by wrong bonds. In the absence of a theory predicting the effects of wrong bonds on the electronic spectra, we cannot draw any firm conclusions from these data concerning their existence. We shall present evidence in Sec. IV D that few wrong bonds exist in these materials.

B. DOVS and bond model

A simple bond model has been used by Weaire and Thorpe[57-59] to account for the qualitative features of the energy states of tetrahedral semiconductors that depend upon nearest-neighbor bond overlap. In this model the basis set for the description of the secular matrix is formed by four hybridized sp^3 atomic valence orbitals pointing from the center to the corners of the tetrahedron (see Fig. 18). The Hamiltonian contains the interaction between orbitals of the same atom and between colinear bonds connecting neighboring atoms. With such an eight-function basis it is possible to describe both the bonding (valence) or antibonding (conduction) states. By adding together the two functions that describe a single bond in the Weaire-Thorpe model, we reduce the basis set to four bonding-type functions which should be able to describe

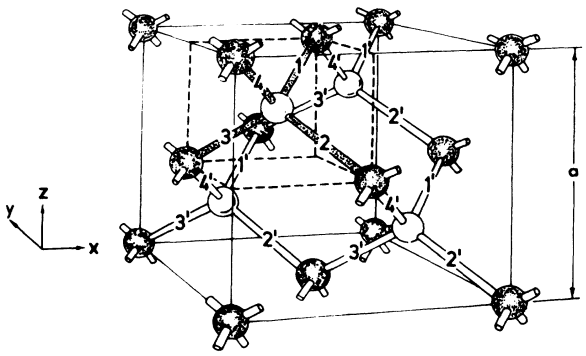

FIG. 18. The zinc-blende unit cell. The white atoms are A-type and the darkened, B-type. The bonds within the primitive cell chosen to lie at the origin are labeled 1, 2, 3, 4, and are shaded. The bonds outside this unit cell are unshaded and labeled with primed numbers.

the valence states under the assumption that they have a predominantly bonding character. A Hamiltonian based on this four-function basis set with the inclusion of nearest neighbor overlap yields for germanium the dashed bands of Fig. 19. The similarity between the "bands" of amorphous materials and those of the crystalline modification follows in this model from the fact that the bond angles and the bond lengths fluctuate only slightly in the amorphous modification. These bands, which are obtained as a solution of a 4×4 matrix, have two serious drawbacks; namely, that the top bands (I) are totally flat, independent of the nearest neighbor interactions parameters, and that the II-III gap at L compared to the total band width is much larger than that obtained in more sophisticated calculations. In the Appendix we show how these drawbacks can be removed without losing the simplicity of the 4×4 Hamiltonian. This is accomplished by introducing an interaction between bonds attached to second-nearest neighbors: The solid curves of Fig. 19 are then obtained. Except for the details of the curvatures of bands I and II at $k=0$, which cannot be reproduced without including antibonding s states (the lowest conduction band) into the Hamiltonian, the solid lines of Fig. 19 represent rather well the valence bands of Ge. A generalization to ionic semiconductors is also possible within the 4×4 framework. The results, which are shown in Fig. 20, exhibit clearly the splitting of the X_1 degeneracy of Ge into $X_1 - X_3$. As shown in Figs. 19 and 20, the binding energies of points L_3' and X_4 (L_3 and X_5 in Fig. 20), measured from the top of the valence band, are always in the ratio 1:2, in agreement with experiment and, to a good approximation, with the Cardona-Greenaway-Hilsum rule mentioned in Sec. IV B.

An interesting conclusion concerning the amorphous materials can be drawn from this band model. We note that the L_1, X_3, and W_2 states of band II are changed very drastically by the introduction of the second-neighbor interaction. In fact, these are the states most susceptible to that interaction. Thus peak II, related to the L_1, X_3, and W_2 states of band II, should be broadened considerably in the amorphous phases as a consequence of the large fluctuations in second-neighbor arrangements (particularly the dihedral rotations) as observed in the experimental RDF's.[35] This conclusion is borne out by our experiments. Also the disappearance of the fine structure of peak I in the amorphous modification can be related to second-neighbor effects which are able to bring the dashed flat bands I (Figs. 19 and 20) to the more realistic solid lines in the crystal.

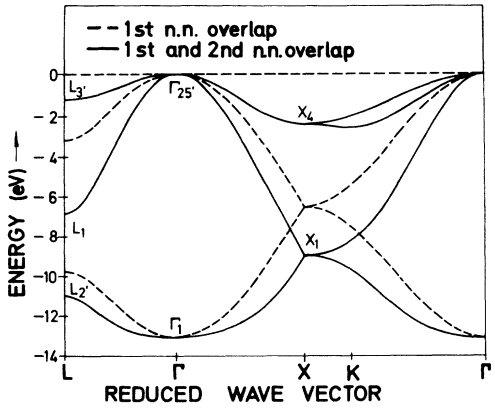

FIG. 19. Valence band structure for Ge calculated with first nearest neighbor overlap (----) and with first and second nearest neighbor overlap (——).

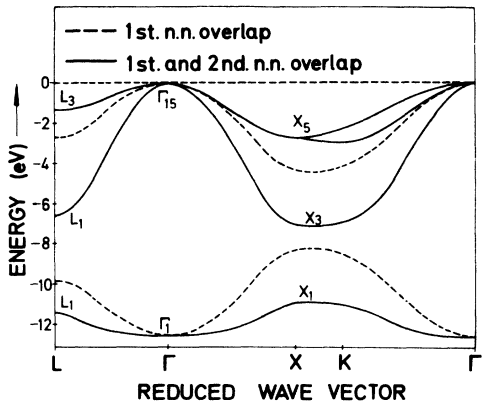

FIG. 20. Valence band structure for a III-V compound calculated with first-nearest-neighbor overlap (----) and with first- and second-nearest-neighbor overlap (——).

In view of this result, we conclude that the smearing of the lower two peaks in the valence bands of Ge may not necessarily be a consequence of the presence of odd-membered rings, as suggested by Weaire and Thorpe.[57-59] The same qualitative differences between the DOVS of the amorphous and crystalline forms of the III-V compounds are also predicted by the theories of Kramer *et al.*,[50-52] although an additional degree of smearing is needed to bring their calculated curves into agreement with both the amorphous and crystalline forms.

C. Core shifts

As already mentioned, the shifts in the core levels between the compound and the constituting elements contain information about the charge distribution and thus the ionicity. Errors in previously reported core shifts owing, e.g., to oxidation, uncertain Fermi levels, etc., have hampered efforts to find a systematic theoretical description of

this effect. We believe the core-level energies presented here are sufficiently accurate to warrant such an effort. As already mentioned, the outermost d level of the cations of the compounds discussed here have been determined by uv photoemission with an accuracy of about ± 0.1 eV with respect to the top of the valence band.

The energies of core levels are obtained automatically in first-principles band calculations (although seldom listed in the corresponding publications!). However, a comparison with experimental results is usually very disappointing even for the very elaborate SCOPW work[22] (Stukel *et al.* give 12.6 eV for the $3d$ levels of Zn in ZnSe, while the experimental value is 10.0 eV).[15] It is therefore useful to resort to simple models which approximate the valence charge distribution to try to describe differences in core energies between elements and compounds. These models, while crude, may at least describe trends in a given class of compounds.

Our model is similar to the electrostatic model used by others to describe chemical shifts of cations.[73-75] Let us consider the valence charge distribution of the cation in its neutral metallic form. Let $a = \frac{1}{2} r$ (r = nearest-neighbor spacing) be the atomic radius. Two extreme spherical models for the charge distribution are possible: The spherical shell of radius a and the uniform volume distribution within a sphere. The corresponding potentials seen by the core for a total valence charge q are for a shell,

$$V_C^A = 2q/r; \tag{1}$$

for a sphere,

$$V_C^B = 3q/r. \tag{2}$$

The corresponding energy shifts on a core level are obtained by multiplying Eqs. (1) and (2) by the electron charge e. Since neither the shell nor the sphere, but rather something intermediate corresponds to the true valence charge distributions in an atom, it is convenient to treat the case of a thick uniform-charge shell lying between radii Γr and r. The corresponding core shift is then given by

$$\Delta E_C(\Gamma) = (3eq/r)A(\Gamma), \tag{3}$$

where

$$A(\Gamma) = (1-\Gamma^2)/(1-\Gamma^3).$$

While the geometrical factor Γ can vary between zero [Eq. (2)] and 1 [Eq. (1)], inspection of the typical atomic charge distributions[76] suggests the reasonable value $\Gamma \cong 0.5$.

For $\Gamma = 0.5$ we obtain

$$E_C(\Gamma = 0.5) = 2.6eq/r. \tag{4}$$

When the metallic atom forms an ionic compound a charge Δq is transferred to the nearest anion at a distance R away. The electrostatic effect on the cation core of these displaced charges is represented by the Madelung constant α, through the expression

$$E_M = \Delta q e \alpha / R. \tag{5}$$

We therefore find for the cation core shift,

$$E_C(\Gamma) = \Delta q e \left(\frac{A(\Gamma)}{r} - \frac{\alpha}{R} \right), \tag{6}$$

a formula similar to that given by Nordberg *et al.*[73] Thus the core shift is given in terms of a geometrical term $A(\Gamma)$, which can be estimated as indicated above, and a charge transfer Δq which can be estimated from Phillips's ionicity scale.[77] From Ref. 77 we find that the total valence charge on the cation of zinc-blende-type semiconductor is

$$q_C = 4e(1 - f_i), \tag{7}$$

where f_i is the ionicity defined by Phillips.[77] If the valence charge of the neutral cation is Z, the charge transfer in the compound is

$$\Delta q = Z - 4(1 - f_i)e. \tag{8}$$

Combining Eqs. (8) and (6) the cation core shift becomes

$$\Delta E_c(\Gamma) = [Z - 4(1 - f_i)]\, e^2 [A(\Gamma)/r - \alpha/R]. \tag{9}$$

We wish to stress that Eq. (9) is only good for the shifts referred to the vacuum level. It is inappropriate to use it to predict the shifts with respect to the midgap or to the top of the valence band since these points may shift too in the compounds.

By similar arguments we find that the shifts for the anion with respect to its elemental form is given by

$$\Delta E_a(\Gamma) = -[Z - 4(1 - f_i)] e^2 \left(\frac{A(\Gamma)}{r_a} - \frac{\alpha}{R} \right), \tag{10}$$

where now r_a is the effective size of the charge sphere added to the anion and $A(\Gamma)_a$ is the geometrical factor describing the shape of its charge distribution. We can expect the simple model to be less accurate for the anions for two reasons: We have the difficulty in estimating the size and shape of the charge sphere added. Also the large number of electrons around the anion can polarize (i.e., expand or contract) to offset the effects of the added charge in changing the positions of the core levels. Obviously this effect would be more difficult to handle; we are therefore presently not discussing the anion shifts since available experimental data (x-ray instead of uv) are not as good as for the cations. For the cation, which has fewer outer electrons, we expect polarization effects to be small.

The interatomic spacings, the Phillips ionicity,[77] and the charge transferred from the cation to the

TABLE VII. Average interatomic spacing, Phillips ionicity f_i, Phillips charge transfer Δq_i, and W, the sum of electron affinity and energy gap for the materials considered here.

Material	r (Å)	f_i	Δq_i	W (eV)
AlSb	2.62	0.426	0.71	5.3[a]
GaP	2.36	0.374	0.50	4.4[a,b]
GaAs	2.44	0.310	0.24	5.5[c]
GaSb	2.62	0.261	0.045	4.8[c]
InP	2.54	0.421	0.69	5.7[c]
InAs	2.62	0.357	0.47	5.3[c]
InSb	2.80	0.321	0.27	4.8[c]
ZnSe	2.44	0.676	0.70	6.8[d]
ZnTe	2.63	0.546	0.18	5.8[d]
CdS	2.52	0.685	0.72	7.2[d]
CdSe	2.62	0.699	0.79	6.6[d]
CdTe	2.80	0.675	0.69	6.2[d]
HgS	•••	•••	•••	5.9[d]
HgSe	2.62	0.65	0.66	5.5[d]
HgTe	2.80	0.68	0.72	5.9[d]
Al	2.86			4.20[c]
Ga	2.71			4.12[c]
In	3.33			4.08[c]
Zn	2.78			4.24[c]
Cd	3.13			4.1[c]
Hg	3.23			4.5[c]

[a]Present work (estimated from low-energy cutoff tails in uv data).

[b]Value is believed to be too low because of phase separated Ga metal.

[c]A. H. Sommer, *Photoemissive Materials* (Wiley, New York, 1968).

[d]Reference 15.

anion as given by Eq. (8), are listed in Table VII. Also listed are the average interatomic spacing for the cation metals used in the calculations. We first note that the charge transfer for the III-V compounds is ~0.4, and for the II-VI compounds, ~0.6. The most notable exceptions are GaSb and ZnTe for which the charge transfer nearly vanishes. This occurs because each of these materials has, according to Phillips, [77] an ionicity which is close to charge neutrality ($f_i = 0.25$ for III-V compounds and $f_i = 0.50$ for II-VI compounds).

In Table VIII we have listed the core shifts determined relative to the tops of the valence bands ($E^{\Gamma VB}$) and with respect to the vacuum level (E^V). Also listed are the shifts predicted by the cation charge models A, B, and C, corresponding to $\Gamma = 1$, 0, and $\frac{1}{2}$, respectively.

The shifts found by referencing all levels to the top of the valence band are small and negative for the Ga compounds, small and positive for the In compounds, large and positive for the Zn and Cd II-VI compounds, and large and negative for the Hg salts. The positions of the Hg 5d level in its metallic form, obtained from the old listing of Bearden and Burr, [78] is believed to have a much larger uncertainty (±1.0 eV) than the others (±0.1 eV).

The scatter in the signs of the shifts clearly indicates the inadequacy of using the top of the valence band to find the core shifts. In each case, we expect the cation to give up charge to the anion, so that its levels should decrease in energy (become more tightly bound). However, it is possible that the geometrical factor can become negative, leading to a chemical shift of a sign opposite to that expected from the charge transfer (in model A, such a scatter in signs occurs). Referring the core levels to the vacuum level, all shifts do indeed become negative, the smallest being −0.7 eV for InSb and the largest being −3.70 eV for HgTe. Upon comparing the curve shifts predicted by the three charge models we find that C most accurately describes the In, Zn, and Cd compounds. For Hg, B gives a better agreement. Because of the large uncertainty in the position of the core level of the metallic Hg, [78] we shall not pursue the question further. We point out, however, that the models do explain the observed greater shift of the core level of HgTe compared to HgSe. The geometrical factors were primarily responsible for this since the charge transfer is about the same for each compound.

The anomalously small predicted shifts for GaSb are a consequence of the small charge transfer predicted by Phillips's ionicity. To bring experiment and model C into agreement with theory, requires that the ionicity of GaSb be increased to ~0.3, or by only ~12%. This demonstrates the potential of photoemission for determining ionicities since it is highly sensitive to deviations away from ionicity values corresponding to neutral atoms.

D. Core levels in amorphous material

The sharp core-level spectra observed in the amorphous materials appear to be in contradiction with what one would expect from a CRN model. In the CRN models that have been constructed so far, nearly every atom participates in a five-membered ring, [36,37] and thus it is always in or very near a wrong-bond pair. As discussed in Sec. IV C, one term contributing to the core shift is the Madelung energy, which can be written

$$E_i^M = \sum_{j \neq i} \frac{eq_j}{R_{ij}}, \tag{11}$$

where E_i^M refers to atom i, R_{ij} is the separation between atoms i and j, and q_j is the charge on atom j. In the crystalline form, E_i^M is a constant for cations and anions, but in an amorphous material there is no reason to expect this term to be a constant for each type of atom. It is well known that the Madelung sum given in Eq. (11) is very slowly converging and should thus be sensitive to the local

structure. For example, in a typical III-V compound with a charge transfer of $\frac{1}{2}e$ and a nearest-neighbor separation of 2.5 Å, a single-nearest-neighbor contribution is 2.5 eV. A wrong bond can be simulated by reversing the sign of the charge of a nearest-neighbor leading to a change in the energy of the core level by twice this amount. For those atoms participating in the wrong bonds, we expect their core levels to be split away from the main spectra. Since Coulombic terms fall off slowly as $1/r$, a random distribution of charge should produce a smearing of the core-level spectra of the more distant neighbors. Since we found that the spectra in the amorphous form are as sharp as in the crystalline form, we conclude that the Coulombic fluctuations in amorphous III-V and II-VI compounds are very small, and thus few wrong bonds are present. However, we cannot rule out the unlikely possibility that the charge in the amorphous form is rearranging itself in such a way as to keep the core levels at a constant value, in spite of any wrong bonds in the structure. We wish to stress that our experimental resolution for the cation levels is 0.1 eV; thus any rearrangement of charge would have to be so precise to prevent the core levels from broadening by more than 0.2 eV, which, if so, is truly remarkable. The lack of additional broadening in the core-level spectra in these amorphous materials rules out the fluctuating potential model proposed by Fritzche.[79] We suggest that similar experiments be performed on chalcogenide glasses to investigate the validity of this model for them.

Even if there are no wrong bonds present, the fluctuations in the distances between near neighbors should cause a smearing of the core-level spectra. While the nearest neighbor separations are well defined, the RDF's show that the second neighbors are distributed over a range of ± 0.5 Å about their average value. It is easy to show that for $q \sim \frac{1}{2}e$,

TABLE VIII. Energy shifts are of the cations (in eV) with respect to their position in the metallic form ΔE^{TVB} and E^{V} are shifts referred to the top of the valence band and vacuum level, respectively. Also included are the core shifts calculated for various model charge distributions (see text).

Compound	ΔE^{TVB}	ΔE^{V}	A ($\Gamma = 1$)	B ($\Gamma = 0$)	C ($\Gamma = \frac{1}{2}$)
AlSb	−0.2	−1.8	−0.30	−2.75	−1.64
GaAs	−0.3	−1.7	−0.22	−1.41	−0.90
GaSb	−0.4	−1.1	−0.06	−0.29	−0.196
InP	+0.05	−1.6	+0.39	−2.49	−1.12
InAs	+0.25	−1.0	+0.15	−1.77	−0.93
InSb	+0.05	−0.7	−0.017	−1.17	−0.69
ZnSe	+0.81	−1.65	−0.43	−3.85	−2.48
ZnTe	0.37	−1.19	−0.24	−0.86	−0.67
CdS	+1.54	−1.56	+0.11	−2.98	−1.65
CdSe	+1.16	−1.34	−0.12	−3.50	−2.1
CdTe	+0.66	−1.44	−0.52	−3.50	−2.2
HgS	−0.64	−3.04	...	...	...
HgSe	−1.91	−2.91	+0.06	−2.46	−1.35
HgTe	−2.30	−3.70	−0.321	−3.37	−2.08

and for completely uncorrelated second-neighbor fluctuations that the core-level spectrum should be smeared by

$$\Delta E_{\mathrm{rms}} = 0.8 \text{ eV}!$$

This value is much larger than observed. Apparently, the second neighbors have a high degree of correlation to maintain a much smaller ΔE_{rms}. Again, the charge in the amorphous form might be rearranging to keep the core levels of the cations and the anions at a constant value. If indeed this is the case, then the solution of Eq. (11) with constant values for cation and anion shifts would give the charge distribution in the amorphous solid. This would make an interesting exercise for the CRN models.

E. Spin-orbit splitting of 4*d* levels

Table II shows a systematic increase in the spin-orbit splitting of the 4*d* levels of In in going from the compounds (0.80 eV) to the metallic In (0.91 eV). This increase is even more spectacular, in the II-VI compounds (Cd metal splitting 0.96 eV, CdTe, 0.63 eV).[15] We note that the spin-orbit splitting of atomic Cd is 0.7 eV, from spectroscopic data,[80] and is close to that in the compound but smaller than that in metallic Cd. We therefore postulate an increase in the spin-orbit splitting of the 4*d* levels of metallic Cd with respect to the isolated atom. This increase can come about through wave-function compression imposed by the boundary conditions in the solid, or similarly, through an apparent effect of the crystal field and the interaction between the *d*-levels of neighboring atoms. This last effect would be expected to be smaller in the compound because of the larger distance between atoms of the same kind.

In Table II of this paper and in Table III of Ref. 15, we see a systematic increase in the 4*d* splitting with increasing lattice constant (i.e., with decreasing ionicity). One could speculate that this effect is due to an admixture of the *p* levels of the valence band to the *d*-core levels. The opposite effect, a small admixture of *d*-core levels to the *p*-levels of the valence band, has been known for some time, to decrease the spin-orbit splitting of the Γ_{15} valence band.[71]

V. CONCLUSIONS

The density of valence states of the amorphous III-V and II-VI compounds are broadened versions of their crystalline counterparts as predicted by Kramer, Maschke, and Thomas.[50–52] We believe this to be due to the similarities in the short range order, especially in the types or rings, of the amorphous and crystalline forms. The importance of the contributions of second-neighbor bond overlap to the electronic spectrum have been investi-

gated with a four-function basis set. These results show that the second-neighbor bond overlap causes shifts as large as 4 eV in the band structures calculated with only nearest-neighbor overlap, and thus the uncertainties in the second neighbor positions can cause the observed smearing in the DOVS of the amorphous form.

We have found that the chemical shifts of the cation can be determined from a simple point-ion model using the Phillips[77] ionicity scale to compute the charge transfer.

The sharp core-level spectra observed in the amorphous forms show no evidence for the Coulombic fluctuations expected from a random network with wrong bonds. The structural model most consistent with the structural and photoemission experiments is a random network lacking the odd-membered rings and having essentially perfect chemical ordering. We suggest that structural models be attempted which fit these requirements. We also suggest that theoretical efforts be devoted to examine the influence of wrong bonds on the valence states and core shifts to verify further our present interpretations which have been deduced by possibly grossly oversimplified assumptions.

ACKNOWLEDGMENTS

We are indebted to G. Krutina for his help in making the measurements. Useful discussions with Dr. P. Thomas, Dr. H. Overhof, Dr. D. Weaire, and Dr. M. Thorpe are gratefully acknowledged. We thank Dr. D. Eastman, Professor D. A. Shirley and their co-workers for preprints prior to publication and Professor Mehlhorn for a discussion concerning the spin-orbit splitting of atomic Cd. We also thank Professor K. S. Song for correspondence concerning our bond-charge model.

APPENDIX: SIMPLE MODEL FOR VALENCE BANDS OF GROUP-IV AND -III-V COMPOUNDS

In this Appendix, we outline a simple band model which seems to give reasonable results for the electronic valence bands of zinc-blende materials with a four-function basis set. The model proposed by Weaire and Thorpe,[57-59] except for the δ function p-like bonding bands (I) gives a fair description of the valence bands but a poor description of the conduction bands. The failure to describe the conduction band states is due to the neglect of the higher-lying atomic orbital states present in the region of the conduction band. Since there are no orbital states in the region of the valence band other than one s and three p levels per atom, we might expect to obtain a good description of the valence bands with a four-function basis set which represents the bonding charge and with the inclusion of more-distant-neighbor overlap. The inclusion of more distant overlap, as shown by Henderson and Ortenburger,[61] should permit the undesirable flat bands found in the Weaire-Thorpe model to be broadened, while at the same time, by reducing the number of basis functions to four, we retain a similar simplicity. The basis set used here is the same as that used by Hall[81] to treat the valence bands of group IV materials. Our contributions are to extend it to the III-V compounds and to introduce more-distant-neighbor overlap.

The zinc-blende structure consists of two interpenetrating fcc lattices displaced along a body diagonal. On one fcc lattice, the atoms are A type and on the other they are B type. The model basis set is shown in Fig. 18; it consists of a glob of bonding charge connecting two atoms A and B.

The atoms serve as vertices at which the bonds overlap. It is easy to identify which bonds are equivalent, since all equivalent bonds point in the same direction. The bonds labeled 1, 2, 3, and 4 point in the $[111]$, $[1\bar{1}\,\bar{1}]$, $[\bar{1}1\bar{1}]$, and $[\bar{1}\bar{1}1]$ directions, respectively. The bonding charge may be constructed by connecting two hybridized sp^3 tetrahedral bonds, pointing along a line connecting nearest-neighbor atoms, so that the charge density is nonvanishing midway between the bonds. This bond has a solely bonding character and we cannot hope to describe accurately the conduction bands or portions of the valence bands that have a large nonbonding character. The antibonding functions can be constructed by choosing the signs of the two sp^3 bonds emanating from nearest-neighbor atoms such that the charge density vanishes midway between them. It has been shown that the valence bands of Ge and Si have a predominantly bonding character, so that the neglect of the antibonding functions may still be a good approximation.[57]

The secular equation for this four-function basis set has the form

$$\begin{vmatrix} E_1 - E & V_{12} & V_{13} & V_{14} \\ V_{12}^* & E_2 - E & V_{23} & V_{24} \\ V_{13}^* & V_{23}^* & E_3 - E & V_{34} \\ V_{14}^* & V_{24}^* & V_{34}^* & E_4 - E \end{vmatrix} . \tag{A1}$$

Including first- and second-neighbor bond overlap, the matrix elements become:

$$\begin{aligned} E_1 &= 2V_2[\cos(k_x + k_y) + \cos(k_x + k_z) + \cos(k_z + k_y)], \\ E_2 &= 2V_2[\cos(k_z + k_y) + \cos(k_y - k_x) + \cos(k_z - k_x)], \\ E_3 &= 2V_2[\cos(k_z + k_x) + \cos(k_x - k_y) + \cos(k_y - k_z)], \\ E_4 &= 2V_2[\cos(k_y + k_x) + \cos(k_x - k_z) + \cos(k_z - k_y)], \\ V_{12} &= V_1^A + V_1^B e^{i(k_z + k_y)} + 2V_2'[\cos(k_x + k_z) + \cos(k_y + k_x)], \\ V_{13} &= V_1^A + V_1^B e^{i(k_x + k_z)} + 2V_2'[\cos(k_x + k_y) + \cos(k_y + k_z)], \\ V_{14} &= V_1^A + V_1^B e^{i(k_x + k_y)} + 2V_2'[\cos(k_z + k_y) + \cos(k_x + k_z)], \end{aligned} \tag{A2}$$

$$V_{23} = V_1^A + V_1^B e^{i(k_x - k_y)} + 2V_2'[\cos(k_z + k_y) + \cos(k_z - k_x)],$$
$$V_{24} = V_1^A + V_1^B e^{i(k_x - k_z)} + 2V_2'[\cos(k_z + k_y) + \cos(k_x - k_y)],$$
$$V_{34} = V_1^A + V_1^B e^{i(k_y - k_z)} + 2V_2'[\cos(k_x + k_z) + \cos(k_x - k_y)].$$

The parameters V_1^A and V_1^B correspond to nearest-neighbor overlap occurring on A-type and B-type atoms, respectively. The best agreement with the more elaborate calculations[23] occurs when we set $V_2' = 0$ and $V_2 > 0$. This approximation can be understood in terms of the directionality of the bond charge. For an sp^3 hybridized orbital, the forward and backward directions have a higher charge density than directions nearly perpendicular to the bond direction. The off-diagonal elements are those arising from bonds that are nearly perpendicular to one another. (It has been pointed out to us by Song[82] that our second-neighbor bond interaction is equivalent to including π bonding between the bonding charges. When we disect our bonding charges into s, p atomic functions, our second-neighbor bond overlap is equivalent to π bonding between orbitals lying on *nearest-neighbor atoms*.) Assuming $V_2' = 0$, the secular equation becomes

$$\begin{vmatrix} E_1 - E & V_1^A + V_1^B e^{i(k_z + k_y)} & V_1^A + V_1^B e^{i(k_x + k_z)} & V_1^A + V_1^B e^{i(k_y + k_x)} \\ V_1^A + V_1^B e^{-i(k_z + k_y)} & E_2 - E & V_1^A + V_1^B e^{i(k_x - k_y)} & V_1^A + V_1^B e^{i(k_x - k_z)} \\ V_1^A + V_1^B e^{-i(k_x + k_z)} & V_1^A + V_1^B e^{i(k_y - k_x)} & E_3 - E & V_1^A + V_1^B e^{i(k_y - k_z)} \\ V_1^A + V_1^B e^{-i(k_y + k_x)} & V_1^A + V_1^B e^{i(k_z - k_x)} & V_1^A + V_1^B e^{i(k_z - k_y)} & E_4 - E \end{vmatrix} . \tag{A3}$$

With the top of the valence band taken as the point of zero energy along Δ, the four solutions are

$$E = 4V_2[\cos(k_x) - 1] \quad \text{(twofold)}$$
$$= +2(V_1^A + V_1^B) \pm 2\,|\,V_1^A + V_1^B e^{ikx}\,| + 4V_2[\cos(k_x) - 1]. \tag{A4}$$

Along Λ ($k_x = k_y = k_z$) the solutions are

$$E = 2V_2[\cos(2k_x) - 1] \quad \text{(twofold)}$$
$$= \frac{E_1 + E_2 + 2(V_1^A + V_1^B) \pm [(E_1 - E_2)^2 + 12\,|\,V_1^A + V_1^B e^{2ikx}\,|^2\,]^{1/2}}{2} \tag{A5}$$

where,

$$E_1 = 6V_2[\cos(2k_x) - 1], \quad E_2 = 4V_2[\cos(2k_x) - 1] + 2(V_1^A + V_1^B).$$

For a compound semiconductor the splitting of the II-III bands at X is:

$$4\,|\,V_1^A - V_1^B\,|$$

proportional to the difference in the potentials of atoms A and B. For group-IV material $V_1^A = V_1^B = V^0$. In this limit, the connection to the Hamiltonian of Weaire and Thorpe becomes apparent. We can obtain the off-diagonal terms of (A3) the same result from their Hamiltonian by adding together the matrix elements of the two functions that describe our single bond.

As shown in Fig. 19, without second-neighbor overlap ($V_2 = 0$), we obtain the flat p-like bands that were also obtained by Weaire and Thorpe.[57-59] The lower portions, arising from an admixture of the s and p levels, give the qualitative features of the band structure calculated by Herman *et al.*[23] The separation between the L_2 and L_1 levels is equal to one-half of the total bandwidth, which, however, is too large. The L_2', L_1, and X_1 points are too high in energy.

By including the second-neighbor bond overlap, maining regions of the band structure are affected little by the antisymmetric potential. The II-III gap and the corresponding peaking of density of states at both sides of the gap, appear clearly in the density of states calculated with our model for the antisymmetric case (Fig. 22). The upper bands (I) are not affected by the antisymmetric part of the potential, and depend solely on the second-neighbor overlap parameter. More elaborate pseudopotential calculations have shown that those bands are similar for all diamond and zinc-blende materials, but seem to undergo compressions with increasing ionicities and lattice constants. The observed constancy of these widths, as postulated by the Cardona-Greenaway-Hilsum rule, is interpreted in the context of this model as a constant second-neighbor overlap parameter. We have no explanation of why this parameter should remain a constant for such a large number of materials other than to conjecture that the spacial extent of the wave function is the same in all compounds.

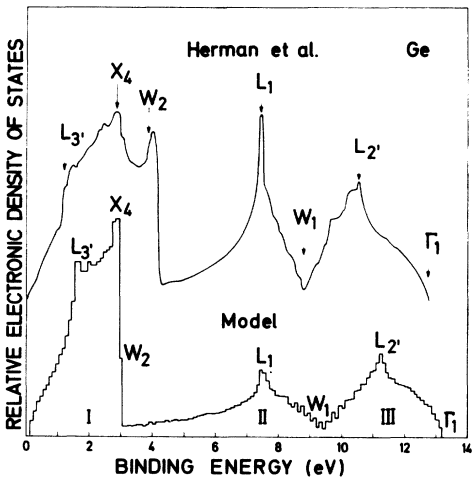

FIG. 21. Density of valence states of cubic germanium for valence bands shown in Fig. 19, compared to that of Herman *et al.* (Ref. 23).

the band structure is significantly improved, as shown by the solid line in Fig. 19. The top of the valence band was, in all cases, chosen to have zero energy. With respect to this origin, the energies of the Γ, X, and L points are

$$L_3' = 4V_2, \qquad \Gamma_1 = +8V_0,$$

$$L_1 = +2V_0 - 12V_2, \qquad X_4 = -8V_2,$$

$$L_2' = 6V_0 - 4V_2, \qquad X_1 = +4V_0 - 8V_2.$$

The bandwidth is given by $+8V_0$, which also represent the atomic s-p splitting. The width of the upper portions of the valence bands, which are now quite realistic in contrast to the flat bands of the Weaire-Thorpe model, are determined primarily by V_2. The ratio of binding energies of the X_5 to that of the L_3 point is 2, in agreement with the Cardona-Greenaway-Hilsum rule. This remains valid even when $V_2' \neq 0$. The agreement with Herman's calculation[23] is not as good in the Σ direction where the lower p band lies about 1-eV deeper at K than it does here. Inspection of $\vec{k}\cdot\vec{p}$ wave functions shows that this level is being repelled by the upper-antibonding p functions, which we have neglected. However, a splitting along Σ does occur even within the limitations of such a small basis set. The X_1, L_1, and L_2' levels and the L_2'-L_1 separation is also brought into better agreement with Herman's calculations.[23] Weaire and Thorpe have shown that even with the inclusion of antibonding functions, the top bonds remain flat as long as only nearest-neighbor overlap is included. Second-neighbor overlap is important, either by implementing a mixture of the bonding-antibonding p-like functions or by contributions to the self-energy, such as we have included.

The density of states calculated with this Hamiltonian by diagonalizing it at 12 000 points in the irreducible zone is compared in Fig. 21 to that calculated by Herman *et al.*[23] As expected from the similarities in the band structures, the density of states of the model exhibits the three main peaks I, II, and III, in fair agreement with those of Herman *et al.*[23] The largest discrepancy with the more exact curve is in the detailed shape of peak I. While we are able to fit the X and L points, we are unable to explain accurately the regions coming from the K and W regions. As mentioned, this discrepancy probably arises from our neglect of the antibonding functions which contribute significantly to this region.

Equation (A3) yields for $V_1^A \neq V_1^B$ the band structure of a zinc-blende compound as shown in Fig. 20 for $V_1^A + V_1^B = 2V_0$ (so as to have the same symmetric potential as for Ge). This figure shows the opening of the gap at X between bands II and III. The remaining regions of the band structure are affected little by the antisymmetric potential. The II-III gap and the corresponding peaking of density of states at both sides of the gap, appear clearly in the density of states calculated with our model for the antisymmetric case (Fig. 22). The upper bands (I) are not affected by the antisymmetric part of the potential, and depend solely on the second-neighbor overlap parameter. More elaborate pseudopotential calculations have shown that those bands are similar for all diamond and zinc-blende materials, but seem to undergo compressions with increasing ionicities and lattice constants. The observed constancy of these widths, as postulated by the Cardona-Greenaway-Hilsum rule, is interpreted in the context of this model as a constant second-neighbor overlap parameter. We have no

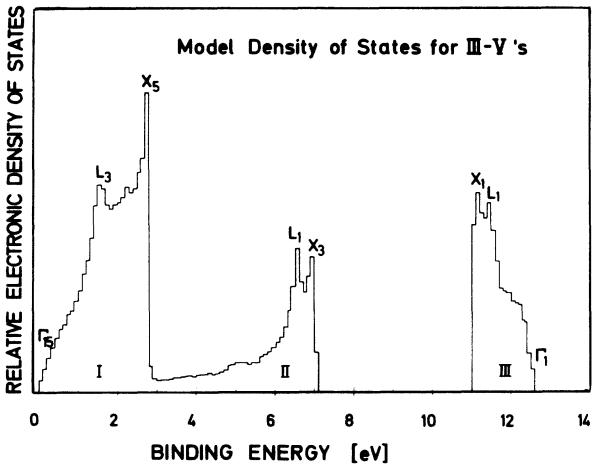

FIG. 22. Density of valence states for the valence bands of the III-V compound shown in Fig. 20.

explanation of why this parameter should remain a constant for such a large number of materials other than to conjecture that the spacial extent of the wave functions is the same in all compounds.

[1]K. Siegbahn, C. Nordling, A. Fahlman, R. Nordberg, K. Hamrin, J. Hedman, G. Johansson, T. Bergmark, S.-E. Karlsson, I. Lindgren, and B. J. Lindberg, *ESCA-Atomic, Molecular and Solid State Structure by Means of Electron, Spectroscopy* (Nova Acta Regiae Soc. Sci. Upsaliensis, Upsala, Sweden, 1967), Ser. IV, Vol. 20.

[2]N. J. Shevchik, J. Tejeda, C. M. Penchina, and M. Cardona, Solid State Commun. 11, 1619 (1972).

[3]R. A. Pollak, L. Ley, S. Kowalczyk, D. A. Shirley, J. D. Joannopoulos, D. J. Chadi, and M. L. Cohen, Phys. Rev. Lett. 29, 1103 (1972).

[4]R. A. Pollak, S. Kowalczyk, L. Ley, and D. A. Shirley, Phys. Rev. Lett. 29, 274 (1972).

[5]W. D. Grobman and D. E. Eastman, Phys. Rev. Lett. 29, 1508 (1972).

[6]M. Cardona, D. W. Langer, N. J. Shevchik, and J. Tejeda, Phys. Status Solidi B 58, 127 (1973).

[7]F. R. McFeely, S. Kowalczyk, L. Ley, R. A. Pollak, and D. A. Shirley, Phys. Rev. B 7, 5228 (1973).

[8]D. E. Eastman and W. D. Grobman, in *Proceedings of the Eleventh International Conference on the Physics of Semiconductors, Warsaw*, 1972 (Polish Scientific, Warsaw, 1972) p. 889.

[9]D. E. Eastman, J. Freeouf, and M. Erbudak, J. Phys. C 6, 56 (1973).

[10]L. Ley, S. Kowalczyk, R. Pollak, and D. A. Shirley, Phys. Rev. Lett. 29, 1088 (1972).

[11]C. J. Vesely and D. L. Kingston, Phys. Status Solidi B 61, 337 (1974).

[12]N. J. Shevchik, J. Tejeda, D. W. Langer, and M. Cardona, Phys. Rev. Lett. 30, 659 (1973); Phys. Status Solidi B 57, 245 (1973).

[13]N. J. Shevchik, J. Tejeda, M. Cardona, and D. W. Langer, Solid State Commun. 12, 1285 (1973).

[14]N. J. Shevchik, M. Cardona, and J. Tejeda, Phys. Rev. B 8, 2833 (1973).

[15]N. J. Shevchik, J. Tejeda, M. Cardona and D. W. Langer, Phys. Stat. Solidi B 59, 87 (1973).

[16]M. Cardona, J. Tejeda, N. J. Shevchik, and D. W. Langer, Phys. Status Solidi B 59, 483 (1973).

[17]J. Tejeda, M. Cardona, N. J. Shevchik, D. W. Langer, and E. Schönherr, Phys. Status Solidi B 58, 189 (1973).

[18]N. J. Shevchik, J. Tejeda, M. Cardona, and D. W. Langer, J. Phys. C 6, 45 (1973).

[19]T. H. Di Stefano and D. E. Eastman, Phys. Rev. Lett. 27, 1560 (1971).

[20]D. E. Eastman and W. D. Grobman, Phys. Rev. Lett. 28, 1378 (1972).

[21]L. F. Wagner and W. E. Spicer, Phys. Rev. Lett. 28, 1381 (1972).

[22]D. J. Stukel, T. C. Collins, and R. N. Euwema, in *Electronic Density of States*, edited by L. Bennett, Natl. Bur. Std. Special Publication No. 323 (U.S. GPO, Washington, D. C., 1971), p. 93.

[23]F. Herman, R. L. Kortum, C. D. Kuglin, and J. P. van Dyke, in *Methods in Computational Physics* (Academic, New York, 1968), Vol. 8, p. 193.

[24]F. Herman and S. Skillman, *Proceedings of the First International Conference on Semiconductor Physics*, Prague 1960 (Academic, New York, 1961), p. 20.

[25]P. Eckelt, Phys. Status Solidi 23, 307 (1967).

[26]F. Herman, R. Kortum, C. D. Kuglin, and J. L. Shay, in II-VI *Semiconducting Compounds*, edited by D. G. Thomas (Benjamin, New York, 1967).

[27]M. L. Cohen and T. K. Bergstresser, Phys. Rev. 141, 789 (1966).

[28]F. H. Pollak, C. W. Higginbotham, and M. Cardona, J. Phys. Soc. Jap. Suppl. 21, 20 (1966).

[29]C. W. Higginbotham, F. H. Pollak, and M. Cardona, in *Ninth International Conference on the Physics of Semiconductors, Moscow* 1968, edited by S. M. Rykin and Yu. V. Shmartsev (Nauka, Leningrad, 1968).

[30]C. Hilsum, *Proceedings of the Seventh International Conference on the Physics of Semiconductors*, Paris, 1964 (Dunod, Paris, 1964).

[31]H. M. Brown and D. E. Brodie, Can. J. Phys. 50, 2502 (1972).

[32]M. Wihl, M. Cardona, and J. Tauc, J. Non-Cryst. Solids 8-10, 172 (1972).

[33]W. Prettl, N. J. Shevchik, and M. Cardona, Phys. Status Solidi B 59, 241 (1973).

[34]D. Weaire and R. Alben, Phys. Rev. Lett. 29, 1505 (1972).

[35]N. J. Shevchik, Phys. Rev. Lett. 31, 1245 (1973) and N. J. Shevchik and W. Paul, J. Non-Cryst. Solids 13, 1 (1973).

[36]D. E. Polk, J. Non-Cryst. Solids 5, 365 (1971).

[37]D. Henderson and F. Herman, J. Non-Cryst. Solids 8-10, 359 (1972).

[38]N. J. Shevchik and W. Paul, J. Non-Cryst. Solids 8-10, 384 (1972) and N. J. Shevchik, Phys. Stat. Solidi B 58, 111 (1973).

[39]N. J. Shevchik and W. Paul (unpublished).

[40]C. H. Drummond (private communication).

[41]J. Stuke, J. Non-Cryst. Solids 4, 1 (1970).

[42]W. Paul, in Ref. 8, p. 38.

[43]G. A. N. Connell and W. Paul, J. Non-Cryst. Solids 8-10, 215 (1972).

[44]W. Eckenback, W. Fuhs, and J. Stuke, J. Non-Cryst. Solids, 264 (1971).

[45]J. Stuke and G. Zimmerer, Phys. Status Solidi B 49, 513 (1972).

[46]W. Gudat, E. E. Koch, P. Y. Yu, M. Cardona, and C. M. Penchina, Phys. Status Solidi B 52, 505 (1972).

[47]M. Cardona, W. Gudat, B. Sonntag, and P. Y. Yu, in *Proceedings of the Tenth International Conference on the Physics of Semiconductors, Cambridge, Mass.*, 1970, edited by S. P. Keller, J. C. Hensel, and F. Stern (U. S. AEC, Oak Ridge, Tenn., 1970).

[48]F. Herman and J. P. van Dyke, Phys. Rev. Lett. 21, 1575 (1968).

[49]D. Brust, Phys. Rev. Lett. 23, 1232 (1969).

[50]B. Kramer, Phys. Stat. Solidi B 47, 501 (1971) Phys. Status Solidi B 41, 649 (1970).

[51]B. Kramer, K. Maschke, and P. Thomas, J. Phys. (Paris) Suppl. 33, C3-157 (1972).

[52]B. Kramer, K. Maschke, and P. Thomas, Phys. Status Solidi B 49, 525 (1972); Phys. Status Solidi B 48, 635 (1971).

[53]T. C. McGill and J. Klima, J. Phys. C 3, 2240 (1970).
[54]J. Keller, J. Phys. C 4, 3123 (1971).
[55]J. Ziman, J. Phys. C 4, 3129 (1971).
[56]J. Keller and J. M. Ziman, J. Non-Cryst. Solids 8-10, 111 (1972).
[57]D. Weaire and M. Thorpe, Phys. Rev. B 4, 2508 (1971).
[58]M. F. Thorpe and D. Weaire, Phys. Rev. B 4, 3518 (1971).
[59]D. Weaire and M. F. Thorpe, in *Computational Methods for Large Molecules and Localized States in Solids*, edited by F. Herman, N. W. Dalton, and T. Koehler (Plenum, New York, 1972).
[60]I. B. Ortenburger, W. E. Rudge, and F. Herman, J. Non-Cryst. Solids 8-10, 653 (1973).
[61]D. Henderson and I. B. Ortenburger, in Ref. 59.
[62]D. Henderson and I. B. Ortenburger, J. Phys. C 6, 631 (1973).
[63]J. D. Joannopoulos and M. L. Cohen, Phys. Rev. B 7, 2644 (1973).
[64]T. M. Donovan and W. Spicer, Phys. Rev. Lett. 21, 1572 (1968).
[65]M. Cardona, C. M. Penchina, N. J. Shevchik and J. Tejeda, Solid State Commun. 11, 1655 (1972).
[66]G. B. Fisher, I. Lindau, B. A. Orlowski, W. E. Spicer, and H. E. Weaver, in Proceedings of the Fifth International Conference on the Amorphous and Liquid Semiconductors, Garmisch-Partenkirchen, 1974 (unpublished).
[67]D. T. Pierce, C. G. Ribbing, and W. E. Spicer, J. Non-Cryst. Solids 8-10, 959 (1972).
[68]D. T. Pierce and W. E. Spicer, Phys. Rev. B 5, 3017 (1972).
[69]L. Ley, R. A. Pollak, F. R. McFeely, S. R. Kowalczyk, and D. A. Shirley (unpublished).
[70]J. Drahokoupil, J. Phys. C. 5; 2259 (1972).
[71]M. Cardona, *Modulation Spectroscopy* (Academic, New York, 1969), p. 242.
[72]M. Cardona and D. L. Greenaway, Phys. Rev. 125, 1291 (1962).
[73]R. Nordberg, R. G. Albridge, T. Bergmark, U. Ericson, J. Hedman, C. Nordling, K. Siegbahn, and B. J. Lindberg, Ark. Kemi 28, 257 (1968).
[74]C. S. Fadley, S. B. M. Hagstrom, M. P. Klein, and D. A. Shirley, J. Chem. Phys. 48, 3779 (1968).
[75]P. H. Citrin, R. W. Shaw, Jr., A. Packer, and T. D. Thomas, in *Electron Spectroscopy* edited by D. A. Shirley (North-Holland, Amsterdam, 1972).
[76]F. Herman and S. Shillwood, *Atomic Structure Calculations* (Prentice-Hall, Englewood Cliffs, N. J., 1963).
[77]J. C. Phillips, Rev. Mod. Phys. 42, 317 (1970).
[78]J. A. Bearden and A. F. Burr, Rev. Mod. Phys. 39, 125 (1967).
[79]H. Fritzche, J. Non-Cryst. Solids 6, 49 (1971).
[80]C. E. More, Atomic Energy Levels, Natl. Bur. Std. Circ. No. 467 (U.S. GPO, Washington, D.C., 1952), Vol. II.
[81]G. G. Hall, Phil. Mag. 43, 338 (1952).
[82]K. S. Song (private communication).